

See discussions, stats, and author profiles for this publication at: <https://www.researchgate.net/publication/378380531>

A review of photocatalytic CO₂ reduction: exploring sustainable carbon emission mitigation from thermodynamics to kinetics and strategies for enhanced efficiency

Article in *Journal of the Korean Ceramic Society* · February 2024

DOI: 10.1007/s43207-024-00365-1

CITATIONS

3

READS

400

10 authors, including:



Muhammad Subhan Javed

University of Lahore

2 PUBLICATIONS 3 CITATIONS

SEE PROFILE



Tehreem Iqbal

Beijing University of Technology

14 PUBLICATIONS 30 CITATIONS

SEE PROFILE



Iftikhar Khan

University of Engineering and Technology, Peshawar

137 PUBLICATIONS 2,011 CITATIONS

SEE PROFILE



Khan Ahmad

22 PUBLICATIONS 216 CITATIONS

SEE PROFILE



A review of photocatalytic CO₂ reduction: exploring sustainable carbon emission mitigation from thermodynamics to kinetics and strategies for enhanced efficiency

Hassan Akbar^{1,3} · Muhammad Subhan Javed² · Syeda Tehreem Iqbal² · Muhammad Iftikhar Khan² · Tauseef Anwar⁶ · Faiza Anjum² · Ashfaq Ahmad⁴ · Muhammad Muneeb² · Asghar Ali² · Won-Chun Oh⁵

Received: 29 October 2023 / Revised: 11 December 2023 / Accepted: 5 January 2024
© The Korean Ceramic Society 2024

Abstract

To mitigate the increased CO₂ emission, CO₂ reduction to multi-carbon fuels or other useable substances is an appealing yet essential approach. Since, reduction of CO₂ is a thermodynamically uphill process, an economical CO₂ fixation is only achievable if energy source used is of renewable energy such as solar energy. Photocatalytic CO₂ reduction is a complex process due to its dependency on catalyst design, selectivity, efficiency, and photostability. The competence of a photocatalytic CO₂ reduction reaction is effected by factors, such as the type of photocatalyst used their band-gap energy, surface area, and structure of the crystal. This review discusses the kinetics and thermodynamics of photocatalytic CO₂ reduction and considers the effects of parameters like defects and impurity doping on photocatalysis. The study also focusses on the selectivity of products, i.e., methane, methanol, formaldehyde, etc. This comprehensive review provides insights into the development and improvement of photocatalytic efficiency for CO₂ photoreduction, contributing to the reduction of carbon emissions and a more sustainable future.

Keywords Photocatalytic CO₂ reduction · CO₂ to fuels · Impurity doping · Kinetic model · Structural defects

Hassan Akbar and Muhammad Subhan Javed have contributed equally to this work.

✉ Asghar Ali
asghar246@gmail.com

✉ Won-Chun Oh
wc_oh@hanseo.ac.kr

¹ Department of Physics, Abbottabad University of Science and Technology (AUST), Abbottabad, Pakistan

² Department of Physics, The University of Lahore, 1-km, Defense Road, Lahore, Pakistan

³ College of Environmental Science and Engineering, North China Electric Power, University 2 Beinong Road, Changning District, Beijing 102206, China

⁴ School of Material Science and Engineering, Shanghai Jiaotong University, Shanghai, China

⁵ Department of Advanced Materials Science and Engineering, Hanseo University, 46, Hanseo Ro, Haemi-myun, Seosan, Chungnam, Republic of Korea

⁶ Department of Physics, Division of Science and Technology, University of Education Lahore, Lahore 54770, Pakistan

1 Introduction

Human activities, particularly the combustion of fossil fuels, such as coal, oil, and natural gas, have markedly increased CO₂ emissions. This surplus of CO₂ intensifies the greenhouse effect, trapping heat within Earth's atmosphere, consequently leading to global warming and alterations in climate patterns. The mitigation of CO₂ emissions stands as a pivotal aspect in addressing climate change and safeguarding the environment [1]. The stability of carbon dioxide arises from its molecular structure and the thermodynamics governing the chemical processes involved—specifically, the carbon–oxygen bonds in CO₂ exhibit notable strength. The formation of this compound releases a substantial amount of energy [2]. To curtail CO₂ emissions, diverse effective strategies exist. These encompass measures, such as transitioning to sustainable energy sources, advocating for energy conservation, adopting cleaner transportation methods, refining waste management practices, and supporting reforestation initiatives. One prevalent method employed for CO₂ reduction is carbon capture and storage (CCS), which involves capturing CO₂ emissions

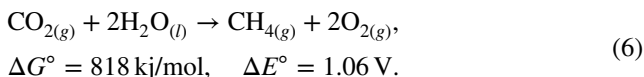
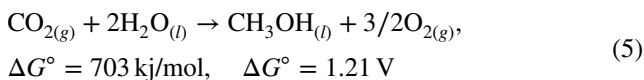
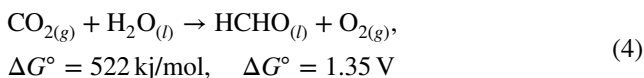
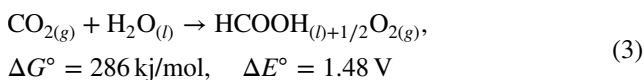
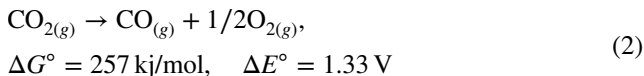
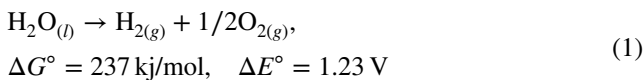
from industrial processes or power generation facilities and subsequently securely storing them underground. Another notable approach is carbon utilization or recycling, wherein captured CO₂ is converted into valuable products such as fuels, chemicals, and construction materials. Furthermore, some researchers are engaged in developing innovative catalysts and processes for the direct conversion of CO₂ into useful chemicals and fuels through electrochemical or chemical reactions [3]. These endeavors are geared toward converting CO₂ from a greenhouse gas into valuable resources, thereby contributing to the reduction of CO₂ emissions and fostering a more sustainable future. Robust research and development in this domain are imperative for combatting climate change and achieving practical carbon management. Another encouraging process known as artificial photocatalytic system (APS), involves photocatalysts, typically semiconductor materials, to harness solar energy for the conversion of CO₂ into valuable products [4]. Catalytic environmental remediation holds paramount importance owing to its potential to expedite chemical reactions crucial to pollutant degradation without being consumed in process. Catalysts act by increasing reaction rates, lowering activation energy and fostering selectivity and specificity toward target contamination. This technology is promising avenue for mitigating CO₂ emission and has the potential to play a crucial role in the transition toward a low carbon future. Photocatalysts can be used for the separation of water molecule into H₂ and O₂ utilizing solar energy for this purpose [5–8]. Photoreduction of CO₂ is of great interest. It is studied globally to overcome the world's energy crises [9, 10]. Researcher are dedicated to develop effective photocatalyst for the conversion of H₂O to molecules and reduction of CO₂ into fuels (H₂, CH₃OH, CH₄, CO, HCHO, and HCOOH) [11]. Photocatalytic CO₂ reduction is more complex due to reasons like selectivity, efficiency, catalyst design, energy requirements, and photostability [12–14]. Due to these reasons, an artificial need for photosynthesis is required which aims to improve the conversion of CO₂ and water. The primary objective behind the development of efficient photocatalyst for water splitting and CO₂ reduction is to harness the abundant and sustainable power of sunlight as a driving force for chemical reaction. This endeavor addresses two critical global challenges: the transition to clean energy sources and reduction of carbon emission. Catalysts that are explored so far are either homogenous or heterogeneous catalysts. Heterogeneous catalysts are in different phase from the reactants, making it easier to separate them from reaction mixture by catalysts' recycling. This reduces the chances of contamination and provides larger surface area for reactants to interact [5, 15–17]. Various semiconductors are used for photoreduction of CO₂ like TiO₂ [18–20], BiVO₄ [21–23], MOFs [24–26], metal halide perovskite [27–29], etc. The photoreduction is basically a surface/interface reaction [30]. The key requirements are needed to be met to effectively utilize the energy from visible-light

spectrum for photocatalytic reaction, which include appropriate band gap [31], photogenerated charge separation [32, 33], selectivity, stability, and activity for existing photocatalytic CO₂ photoreduction. Facilitating the efficient generation of charge carriers through light absorption and subsequent surface reactions are essential aspects of CO₂ photoreduction as they determine the whole efficiency and selectivity of the process in converting CO₂ into valuable fuels or chemicals [4, 34, 35]. Previous research has shown that defects in photocatalytic materials can alter their electronic structure and optical properties [36–39]. These defects could be minimized by doping, enabling the material to absorb a wider range of light and promoting efficient charge separation and reducing recombination rates [40–42]. There is an increasing interest in harnessing CO₂, the most abundant and economically viable carbon-rich resource, for the progress of alternating energy innovation [43]. The concept of utilizing photocatalytic reactions for sustainable solar energy, to transform atmospheric CO₂ waste into alternative fuels, offers a feasible resolution. This innovation strategy not only diminishes carbon dioxide emissions but also concurrently upcycle it as a renewable fuel increasing solar energy resources [44]. Effective photocatalytic performance hinges on various factors, in which the presence of highly efficient photocatalyst stands out as a pivotal determinant. Conversely, optimizing light absorption, minimizing photon losses, and mitigating charge carrier recombination have garnered considerable focus in shaping a more proficient designing of catalyst. The main goal of this review paper is to furnish an extensive literature overview concerning the evolution of various catalysts for conversion of CO₂ to other fuels. In this context, the paper provides a thorough examination of the working mechanism, developmental aspects, and proactive measure aimed at addressing CO₂ photocatalytic reduction. Additionally, it offers insight into future objectives and directions. The overarching aim of this review is to furnish essential background knowledge and outline general research pathways for individuals engaged or intending to enter the domain of CO₂ conversion processes.

2 Thermodynamics of photocatalytic CO₂ reduction

Thermodynamics of CO₂ reduction reaction is found to be contingent on redox potential ΔE° and Gibbs free energy ΔG° [45]. Due to highly positive ΔG° , which indicates that the reaction is endothermic and not favorable under standard conditions, CO₂ reduction is an energetically uphill and non-spontaneous process [46, 47], which means that it requires an input of energy to proceed and it is not favorable for normal temperature and pressure ranges. Compared to water splitting where ΔG° is negative, indicating thermodynamic favorability and spontaneity under standard conditions, CO₂

reduction requires significantly more energy to drive the process. Therefore, the energy storage ratio of CO₂ reduction, i.e., the amount of energy needed for the reaction compared to the energy stored in the resulting products, is generally much higher than that for water splitting [48–50]. The reactions along with the redox potential and Gibbs free energy are given below from Eqs. 1–6 in which Eq. 1 shows the water splitting, while Eqs. 2–6 shows CO₂ reduction [51]



As shown in Fig. 1, the electrons are responsible for CO₂ reduction to convert it into low carbon fuels like CO and HCOOH, while on the other hand, holes in valence band interact with water molecules to produce O₂ [45].

In CO₂ photoreduction, the band gap holds great importance. The photoreduction takes place if the conduction band level is higher than that of reduction potential of CO₂, while valence band on the other hand is more positive than that of oxidation potential [45].

Photocatalytic properties arise when electron and hole charge carriers are generated by absorbing incoming photons with energies equal or greater than that of band gap (E_g). Electrons in conduction band interact with H₂O to produce of H₂ and with CO₂ to produce other useful fuels [7, 16, 53, 54]. Many potential semiconductors have been studied based on this basic principle; some of them are TiO₂ [55, 56], ZnO [57–61], ZnS [61–64], SrTiO₃ [65–68], SiC [57, 69–71], Cu₂O [72–75], CdS [57, 76–81], GaP [57, 82], TaON [83–86], C₃N₄ [87–89], BiVO₄ [90–94], and Ta₃N₅ [95–98]. Among them, TiO₂ has been studied more because of its abundance, stability, photocatalytic activity, low toxicity, and versatility. One other main reason is it being primarily active under UV light due to its wide band gap, which

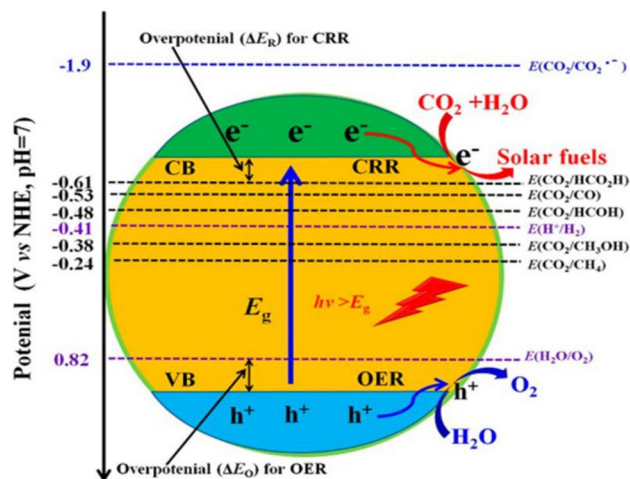


Fig. 1 Representation of CO₂ photoreduction in a semiconductor. Reprinted from [45, 52]

restricts its ability to absorb visible-light wavelength effectively [99–102]. The remaining materials are good photocatalyst for CO₂ photoreduction under visible light. These photocatalysts with more negative CB facilitates electron transfer and promote more efficient CO₂ conversion [4], as shown in Fig. 2.

An electrochemical reaction with higher standard potential is more thermodynamically favorable and tends to proceed in forward direction. Table 1 shows some of the electrochemical reactions with standard potential ΔE° at 25⁰ C temperature and pH kept at 0. These data are further illustrated using graphical plot in Fig. 3. The standard potential provides insight into the spontaneity of the electrochemical process and its feasibility under standard conditions [103, 104].

3 Kinetic study of CO₂ photoreduction

The kinetics of CO₂ photoreduction is well explained by empirically derived Langmuir Hinshelwood model which also leads to micro-kinetic modeling [109]. The advantage of describing heterogeneous catalysis is it provision of insights into reaction mechanism, surface adsorption, the reaction rates at the catalyst surface, and the irradiance. Using this information, the rate of the reaction can be found using Eq. 1 [45]. The major flaw of this LH-based model is that it is time taking and much effort is needed in gathering the CO₂ photoreduction kinetics. Since heterogeneous catalytic reaction is majorly surface reactions, it is essential to determine the moles of reactants consumed or products generated per unit of time and per unit of reaction volume [109], while light is an additional requirement for some catalytic reaction.

Fig. 2 Energy band characteristics in various semiconductors' photocatalysts and the redox potentials of CO₂ reduction in an aqueous solution pH = 7 [4]

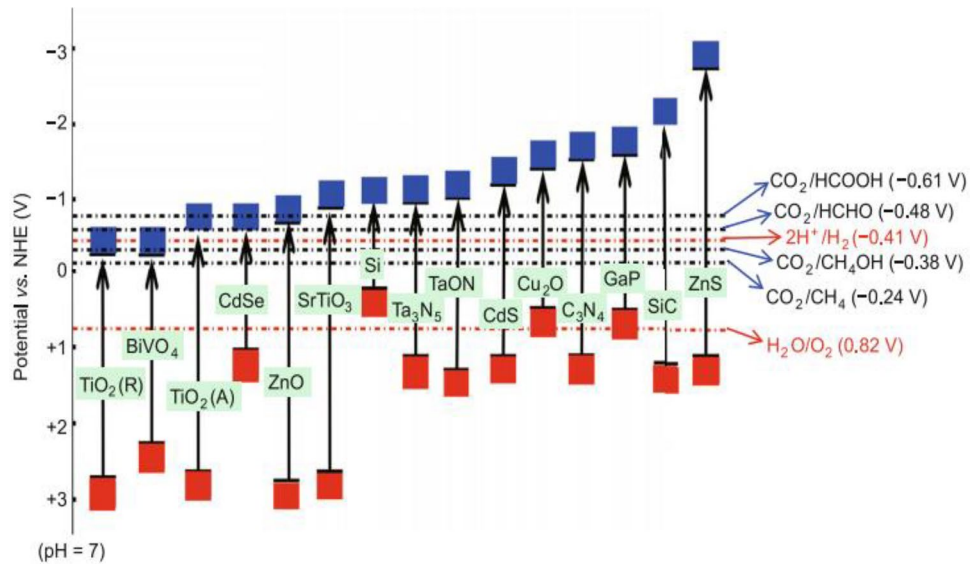


Table 1 Standard potential for CO₂ reduction reaction [49, 105–108]

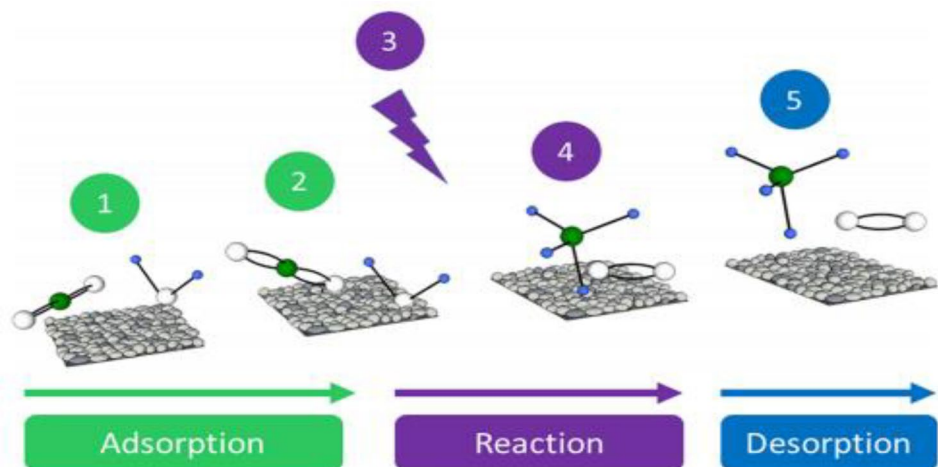
Electrochemical half-reaction	Standard potential ΔE°
$2\text{H}^+ + 2\text{e}^- \rightarrow \text{H}_{2(\text{g})}$	0
$2\text{H}_2\text{O}_{(\text{l})} + 4\text{h}^+ \rightarrow \text{O}_{2(\text{g})} + 4\text{H}^+$	1.229
$\text{CO}_{2(\text{g})} + \text{e}^- \rightarrow \text{CO}_2^-$	-1.9
$2\text{CO}_{2(\text{g})} + 2\text{H}^+ + 2\text{e}^- \rightarrow \text{H}_2\text{C}_2\text{O}_{4(\text{aq})}$	-0.475
$\text{CO}_{2(\text{g})} + 2\text{H}^+ + 2\text{e}^- \rightarrow \text{HCO}_2\text{H}_{(\text{l})}$	-0.2
$\text{CO}_{2(\text{g})} + 2\text{H}^+ + 2\text{e}^- \rightarrow \text{CO}_{(\text{g})} + \text{H}_2\text{O}_{(\text{l})}$	-0.12
$\text{CO}_{2(\text{g})} + 4\text{H}^+ + 4\text{e}^- \rightarrow \text{C}_{(\text{s})} + 2\text{H}_2\text{O}_{(\text{l})}$	0.21
$\text{CO}_{2(\text{g})} + 4\text{H}^+ + 4\text{e}^- \rightarrow \text{HCHO}_{(\text{l})} + \text{H}_2\text{O}_{(\text{l})}$	0.07
$\text{CO}_{2(\text{g})} + 6\text{H}^+ + 6\text{e}^- \rightarrow \text{CH}_3\text{OH}_{(\text{l})} + \text{H}_2\text{O}_{(\text{l})}$	0.03
$\text{CO}_{2(\text{g})} + 8\text{H}^+ + 8\text{e}^- \rightarrow \text{CH}_4_{(\text{g})} + 2\text{H}_2\text{O}_{(\text{l})}$	0.17
$2\text{CO}_{2(\text{g})} + 8\text{H}_2\text{O}_{(\text{l})} + 12\text{e}^- \rightarrow \text{C}_2\text{H}_4_{(\text{g})} + 12\text{OH}^-$	0.07
$2\text{CO}_{2(\text{g})} + 9\text{H}_2\text{O}_{(\text{l})} + 12\text{e}^- \rightarrow \text{C}_2\text{H}_5\text{OH}_{(\text{l})} + 12\text{OH}^-$	0.08
$2\text{CO}_{2(\text{g})} + 13\text{H}_2\text{O}_{(\text{l})} + 18\text{e}^- \rightarrow \text{C}_3\text{H}_7\text{OH}_{(\text{l})} + 18\text{OH}^-$	0.09

By maintaining both of these quantities, we can achieve the desired rate of reaction for CO₂ photoreduction

$$r = kI^\alpha \frac{\prod_{i=1}^n k_i p_i}{(1 + \sum_{i=1}^z k_i p_i)^n} \quad (7)$$

Here, r is the rate of reaction ($\mu\text{mol gcat}^{-1} \text{h}^{-1}$), k is the rate constant ($\mu\text{mol gcat}^{-1} \text{h}^{-1}$), I is the irradiance, α is the reaction order of light intensity (dimensionless), k_i represents the equilibrium adsorption constants for reactants and product (bar^{-1}), p_i refers to partial pressures for reactants and products (bar), n indicates the absorbed reactants that are involved in surface reaction, and z indicates all the reactants and products [45]. Selectivity of catalyst is also based on temperature, because increasing the temperature also enhances the diffusion rate of molecules which directly impacts the rate of reaction [45]. LH-based kinetic model for CO₂ photoreduction is given by Fig. 3 [110–115].

Fig. 3 Illustration of the Langmuir–Hinshelwood (LH)-based kinetic model for CO₂ photoreduction. [Step 1; H₂O and CO₂ diffuse to photocatalyst surface, step 2; molecules migrate within the active sites, step 3; light needed for rate of reaction, step 4; photoreaction start at active sites of two adjacent sites, Step 5; a the desired product is desorbed]



An LH-based model kinetics equation was developed for the gathering of the photoreduction catalysts for carbonate by UV/TiO₂ in aqueous solution [116]. Using UV light and TiO₂ to reduce carbonate in a solution is more effective when the solution is slightly acidic compared to when it is alkaline. The result also indicates that the speed at which this reduction happens increases when you have stronger UV light; however, adding too much TiO₂ actually blocks the UV light from penetrating the solution, as a result, slowing down the reaction [116, 117].

Hence, studies show that the photoreduction of CO₂ is thermodynamically favorable than that of kinetics photoreduction due to the context of multi-electron reduction processes [4]. The efficiency of photocatalytic CO₂ reduction is influenced by factors such as the type of photocatalyst used, their band-gap energy, surface area, and structure of the crystal. Furthermore, several factors including lighting conditions (intensity, wavelength, and duration of illumination), along with reaction condition (temperature, pH), and co-catalyst enhance the photocatalytic efficiency. These factors improve adsorption, enable effective charge separation, and catalyze the conversion of reactants into valuable products. The choice of co-catalyst depends on the specific photocatalyst being used [118]. Basics of photocatalytic process can be summarized as follows:

- (I) Photon is absorbed with sufficient energy which generates e⁻/h⁺ pairs.
- (II) Separation of these charge carries and their transportation from valence band to conduction band.
- (III) The occurrence of the chemical reaction on the surface [7, 119, 120].

The most frequently employed type of light is ultraviolet (UV) light source for photocatalysis, even though only 4% of solar energy is UV light, while 43% is visible light [121–123]. Hence, using narrow band photocatalyst in visible-light spectrum would be more energy efficient [124, 125].

The efficiency of a photocatalytic material can be calculated by its product yield. *R* can be given by

$$R = \frac{n(\text{Product})}{\text{Time} \times m(\text{catalysts})}$$

The common unit for *R* is mol h⁻¹ g⁻¹ for the catalyst, while for the product, it is commonly measured in molar units (μmol) or in concentration units (ppm) [121]. The efficiency of photocatalyst depends upon the amount of photocatalyst, light intensity, the area exposed for their interaction, etc. The product which is formed by the photocatalyst can be measured by their quantum yield [121], using the formula below

$$\text{Overall quantum yield (\%)} = \frac{\text{Number of reactant electron}}{\text{Number of absorbed photon}} \times 100\%$$

$$\text{(App) quantum yield (QY \%)} = \frac{\text{Number of reactant electrons}}{\text{Number of incident photon}} \times 100\%$$

$$\text{(App) quantum yield of CO (\%)} = \frac{2 \times \text{Number of CO molecules}}{\text{Number of incident photons}} \times 100\%$$

$$\text{(App) quantum yield of HCOOH (\%)} = \frac{2 \times \text{Number of HCOOH molecules}}{\text{Number of incident photons}} \times 100\%$$

$$\text{(App) quantum yield of HCHO (\%)} = \frac{4 \times \text{Number of HCHO molecules}}{\text{Number of incident photons}} \times 100\%$$

$$\text{(App) quantum yield of CH}_3\text{OH (\%)} = \frac{6 \times \text{Number of CH}_3\text{OH molecules}}{\text{Number of incident photons}} \times 100\%$$

$$\text{(App) quantum yield of CH}_4\text{ (\%)} = \frac{8 \times \text{Number of CH}_4\text{ molecules}}{\text{Number of incident photons}} \times 100\%$$

As photocatalytic reaction strongly depends upon the photoabsorption, so the photocatalytic activity be contingent with the incident light wavelength. The quantum yield is calculated by calculating the intensity of light and amount of catalyst [126]. Experimental measurements required to determine the quantum yield for a photocatalytic process involving the production of carbon monoxide, formic acid, formaldehyde, methanol, and methane in a photocatalytic reaction are calculated. It is expressed as a percentage and is a measure of the efficiency of the process in converting absorbed photons into the formation of formic acid.

Numerous efforts have been dedicated to find suitable single-phase photocatalyst that can be driven by visible light (CdS [78, 81, 127], C₃N₄ [87, 128, 129], WO₃ [130, 131], CaFe₂O₄ [132], LaCoO₃ [133], BiVO₄ [134, 135], Bi₂WO₄ [136, 137], Fe₂V₄O₁₃ [138], and InTaO₄ [139–142] are active photocatalyst under visible region), and various strategies have emerged in the field of photocatalytic CO₂ reduction. These strategies include techniques like doping, alloying, utilizing surface plasmonic effects, introducing structural defects, sensitization, and forming solid solution [4, 143, 144]. Here, we will discuss two of these strategies, i.e., impurity doping and structural defects.

4 Impurity doping

To enhance the light-driven properties of utilizing semiconductors to enhance the photocatalytic reduction of CO₂, doping is the first strategic process which modulates the arrangement of electrons within a material, optical properties, and surface chemistry of the photocatalyst, leading to improved catalytic activity, selectivity, stability, and reduced energy barriers. Doping can be a versatile and effective strategy to customize the properties of photocatalysts for CO₂ reduction. The success of doping primarily hinges on the choice of dopants, dopants methods, and their potential impact on catalytic performance. Doping can create active sites on catalyst surface that facilitate CO₂ adsorption, activation, and reduction, enabling achievement of two-step photoexcitation using photons with low-energy visible-light spectrum [145, 146]. On the other hand,

nonmetal ion doping can shift the adsorption edge of the catalyst material toward longer wavelengths, enabling adsorption of visible light and that absorption is important for harnessing solar energy [147–149]. Nitrogen and iodine are well-studied material for their red shift optical behavior and they improve the visible-light absorption properties of wide-band-gap semiconductor materials [150]. TiO₂ is considered to be very prominent and potentially studied semiconductor material which has been investigated and developed [151]. Some important parameter for selectivity of the product includes temperature, pressure, and nature of the photocatalyst [152]. On the basis of these parameters, liquid-phase system is preferable. Many up-to-date research efforts have primarily focused on liquid samples, leaving the gas phase largely unexplored. This bias toward liquid-phase studies is often due to analytical limitations, as it is easier to analyze and quantify products in a liquid medium. However, this focus on liquid-phase studies has left the investigation of gas-phase products relatively neglected and less well understood. Gas phase system are reported solar products which are strongly dependent on the photocatalytic process, CO and CH₄ and their metal-doped properties are more functional for their production [153]. Among all metals, platinum (Pt) exhibits favorable results for methane due to higher surface electron density [154, 155]. Similarly, Cu [156], Ag [157], Ni [158], Mg [159], Au [160], Rh [161], and graphene [162] produce methane at a higher quantity in gas phase of CO₂ reduction. While in liquid-phase conversion of CO₂ reduction, the by-product is mostly methanol CH₃OH. Materials like Cu [115, 163], Ag [157], Ni [164, 165], Zn [166], and graphene-based material [167] are mostly studied broadly for their selectivity in photocatalytic CO₂ reduction, and their comparison is shown in Fig. 4.

The doping metal cations are more functional not only for creating space for active oxygen sites in reaction, but they are also for charge separation and adsorption through band-gap states. Contrary to this, we have to limit their concentration, because if dopant concentration increases, it will decrease the activity of photocatalytic CO₂ reduction.

5 Structural defects

Structural defects have crucial role in the photocatalytic CO₂ reduction process. These defects can include vacancies, interstitials atoms, grain boundaries, and other lattice imperfections in a photocatalytic material. Defects can impact the material's electronic structure, surface reactivity, and charge carrier dynamics. All of these factors play a vital role in facilitating the CO₂ reduction reaction. These defects introduce localized energy levels within the band gap of the material, promoting the absorption of a broader range of light wavelengths. An increased light absorption can improve the effectiveness of the photocatalytic process. Moreover, defects

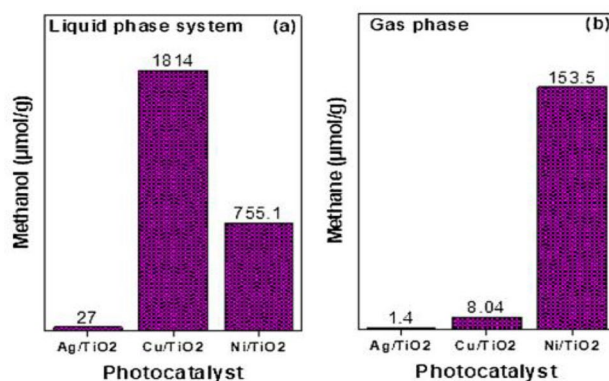


Fig. 4 Phase selectivity products in gas and liquid for CO₂ reduction [115, 152, 157, 160, 168, 169]

can assist as trapping sites for charge carriers, leading to prolonged lifetimes and improved segregation of electrons and holes, which is essential for redox reaction involved in CO₂ reduction. However, excessive defects might lead to an increased recombination of charge carrier, offsetting the beneficial effects [170–172].

Liu et al. [173] performed an investigation on the nanocrystals structure of TiO₂ and found that TiO₂ polymers can exhibit various crystalline configuration including (anatase, rutile, brookite, and TiO₂(B) polymorphs) [174]. It is worth noting that the formation of brookite is relatively infrequent or sporadic [175–177]. The photocatalytic CO₂ reduction is found to follow the sequence anatase > brookite > rutile [4]. Increase in generation of CO and CH₄ from CO₂ photoreduction in the existence of oxygen vacancies provides additional electronic states that can capture charge carriers (e⁻/h⁺) generated upon light absorption. Ti⁺³ species can act as electron donor, and its presence can also influence the charge carrier dynamics and surface activity, leading to an enhanced catalytic activity [173, 178]. Dislocations and grain boundaries are areas of crystal lattice mismatch within a material. These regions can create charge separation and accumulation zones, enhancing the disentanglement of photogenerated electron–hole pairs, as a result, charge carriers can migrate to these regions and participate in CO₂ reduction reaction. Recognizing and addressing these defects through precise material design, controlled synthesis techniques, and innovative surface modification strategies are crucial steps toward maximizing the performance of photocatalytic CO₂ reduction.

Stimulated by the essential researches of CO₂ adsorption and dissociation at defect sites, incredible efforts have been done on the photocatalytic decrease of CO₂ by means of defect-mediated materials. For illustration, the co-exposed (001) and (101) facets of oxygen-deficient TiO₂ nanocrystals were described to accomplish a quantum yield of 0.134% for CO₂ drop to CO underneath the expose of visible light [179,

180]. The electronic structure of catalyst is tuned by defect engineering, which extra advances the photocatalytic activity for the application of CO₂ reduction. For example, the defect-rich BiVO₄ nanosheets were produced and executed in CO₂ photoreduction. In the accumulation of vacancies persuaded by defects, the addition of interstitial and substitutional atoms into material lattice by doping [181]. The exotic atoms can be employed as active sites to alter the adsorption of CO₂ and related intermediates, forming various products. For illustration, it was described that the choosiness of CO₂ reduction could be mostly transformed by acquaint with various single-atom metal sites to g-C₃N₄ matrix.

6 Graphene-based nanomaterials

The initial isolation of graphene occurred and characterized in 2004 [182]. The diverse synthesis methods and distinctive characteristics of nanomaterials based on graphene make them highly favorable contender for the future technologies. Graphene is like a super-thin layer of sheets composed of carbon atom arranged in hexagonal pattern and incredibly thin that its thickness of only 0.334 nm which makes it the slenderest material globally. And because one of a kind properties like larger surface area (~2600 m²/g) [183], higher electron mobility (200,000 cm²/Vs) [184], escalate thermal conduction (3000–5000 Wm/K) [185], maximal optical transparency (97.4%) [186], and possessing remarkable strength characterized by a high young's modulus of 1TPa [187]. A carbon allotrope that exists primarily in a two-dimensional form composed of sp² carbon atom with hybridize orbitals is typically referred to as graphene (Fig. 5) by (Armano and Agnello) [188].

Apart from graphene, reduced graphene oxide (RGO), in addition to pure graphene, can serve as a viable material for CO₂ capture. When considering the production quantity, graphene oxide (GO) which is an intermediate product in graphene synthesis is also a valuable candidate. Between 2014 and 2022 in Fig. 6 [189], there has been remarkable threefold increase in the number of research publication focused on environmentally friendly methods for producing graphene from natural carbon resources.

Regarding the advancement of graphene, there have been significant development as considered a viable element for CO₂ capture application [190]. Graphene-based nanomaterials are the strongest cross-linking systems with strong light absorption and many functional groups. However, mass production of catalysts is still a challenge in terms of morphology, composition, and yield and cost control. This review provides an in-depth discussion of the combination of graphene with other nanomaterials, leading to new nanocomposites that can exhibit good properties such as rapid separation, transport, high surface area, and better CO₂ adsorption level.

For charge transfer method heterojunctions, methods such as type II and type Z are common. In graphene heterojunctions, the graphene itself acts as electron tunneling, changing the Z type to the II type. Therefore, more attention should be paid to the Z shape of graphene-based nanomaterials (Table 2).

7 Summary and categories of graphene-based composite photocatalyst

Table 3 summarizes the graphene-based composite photocatalyst for CO₂ reduction. In summary, the main finding indicates that the graphene-based composite designed for reducing CO₂ through photocatalysis typically involves a combination of graphene and semiconductors. In this setup, semiconductor captures light energy, while graphene serves as a co-catalyst. Furthermore, there are reports indicating that substances derived from graphene, like graphene oxide (GO) and nitrogen-doped graphene, can act like semiconductors. These materials have been shown to effectively use light energy to reduce CO₂. Hence, they can be seen as a different category of photocatalyst based on derivatives of graphene.

The CO₂ transformation process comprises two essential steps: CO₂ capture and subsequent transport to the catalytic site [216, 217]. Porous capture materials are rich in adsorptive sites, yet they exhibit lower catalytic activity for CO₂ reduction compared to semiconductor or precious metals [218, 219]. Hence, the overall photoreduction efficiency is primarily contingent on the transfer of CO₂ from the capture materials to the photocatalyst [220]. Consequently, to attain greater CO₂ conversion rates, an effective photocatalyst must possess both a substantial CO₂ adsorption capacity and minimum diffusion distance. Creating a porous composites structure involves integrating hyper-crosslinked polymers (HCP) onto graphene functionalized with TiO₂ (TiO₂-FG) through an in situ knitting process. The HCPs, which constitute organic microporous materials in their pure form, exhibit a substantial surface area, exceptional CO₂ adsorption capacity, and remarkable physicochemical durability. Notability, this instance represents the integration of microporous organic polymers with photocatalyst for CO₂ conversion, a distractive approach amid the numerous reported photocatalytic methods. The TiO₂-G composite is first obtained through the reduction of graphene oxide (GO), followed by the in situ growth of anatase TiO₂ crystal featuring reactive [32, 215], via solvothermal process [221]. Ultra-thin polymer layer is hyper-crosslinked onto TiO₂-FG by knitting syn-PhPh₃ and connecting them to the open phenyl groups on graphene. This well-defined HCP-TiO₂-FG structure is expected to improve the adsorption capacity for CO₂ due to the enhanced characteristics of HCPs, and the short diffusion distance around the TiO₂ photocatalyst. This structure envisioned to boost

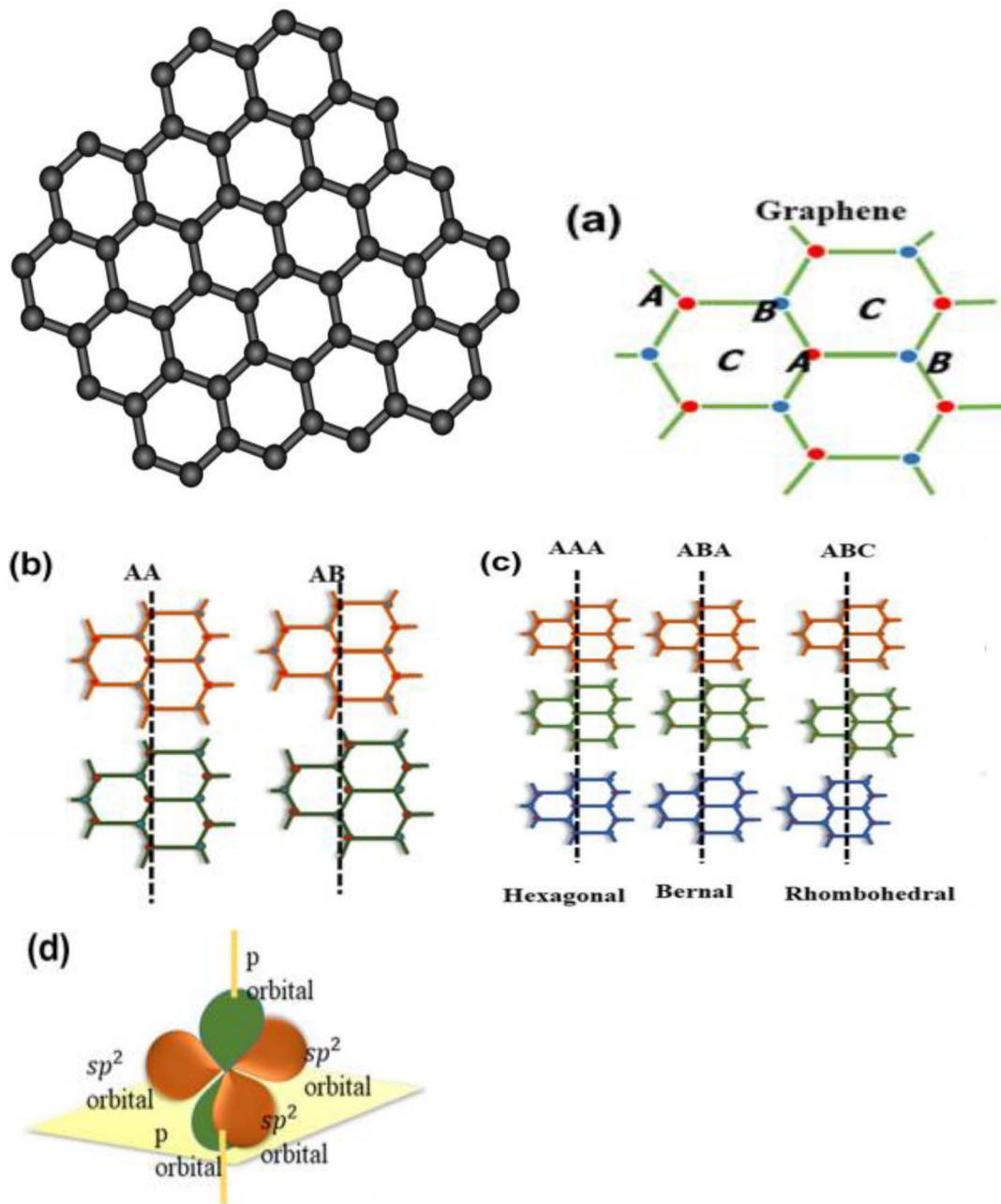


Fig. 5 Two dimensional structure of graphene: **a** SLG structure, A and B sublattice denotes carbon positions, **b** BLG stacking types, **c** TLG stacking types, and **d** π covalent bond and sigma bond arrangement in the hexagonal lattice of graphene [186, 189]

the reactivity of CO_2 molecules, fascinating the production of CH_4 . Well-defined structure is depicted in Fig. 7 [222].

Morphology of as above composites HCP- TiO_2 -FG was inspected by FE-SEM, TEM, and atomic microscopy (AFM). Using FE-SEM analysis, we found that the pure HCPs, produced through our previous knitting technique, displayed structural layering within their bulk composition. In XRD, the samples comprised exclusively of anatase TiO_2 crystals. Incorporating HCPs layer did not induce any change

in the crystal phase of TiO_2 , but it did lead to a noticeable enlargement in the particular size in Fig. 8a, and the surface structure and composition is given by XPS measurement. In contrast to TiO_2 -G, the strength of Ti and O signal peaks in TiO_2 -FG and HCP- TiO_2 -FG gradually diminished, primarily because of TiO_2 content. In high-resolution C1s spectra, the proportion of sp^2 and sp^3 signal exhibits an upward trajectory following the functionalizing and knitting. This change was attributed to an increase in the sp^2 presence in comparison

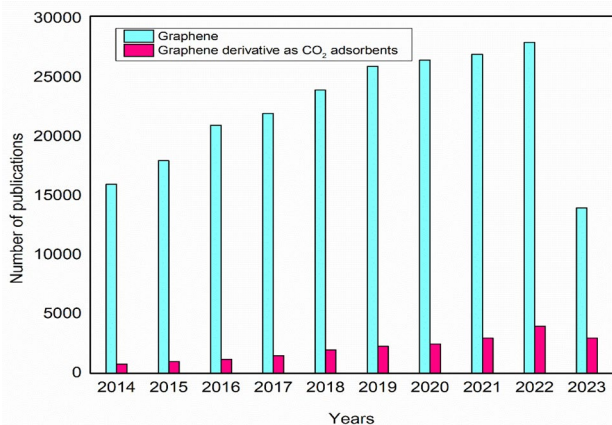


Fig. 6 Publication trends for graphene and its derivative over recent years [189]

to the generation of sp^3 C [223], as shown in Fig. 8b; notably, the peak of Ti2p experienced a shift of approximately (~ 0.2 eV) toward higher energy upon the creation of HCP layers. This electronic conformation shows the interaction between HCP and TiO_2 . FT-IR spectrum of TiO_2 -FG, the FT-IR spectrum of HCP- TiO_2 -FG distantly exhibits pronounced C-H-stretching vibration of methylene around 2920 cm^{-1} and distinctive peaks related to the vibrations of the aromatic ring skeleton at approximately 1485 cm^{-1} [224, 225]. Incorporating phenyl groups into TiO_2 -FG led to the emergence of supplementary peak at 136.7 ppm within the carbon region. This peak was attributed to the functionalization of TiO_2 -G. Additionally, the resonance at 127.2 ppm was assigned to the sp^2 carbon of graphene. The increase intensity of resonance peak around 136.7 ppm can be attributed to the abundant introduction of sp^2 carbon through the process of knitting syn-phph3 with TiO_2 -FG to create HCP- TiO_2 -FG and simultaneously the formation of methylene with new peak at 32.9 ppm Fig. 8c [222]. The composite structure HCP- TiO_2 -FG outstanding thermal stability even at temperature as high $400\text{ }^\circ\text{C}$ due to presence of HCPs layers firmly on graphene. Porosity measurement is shown in Fig. 8d, both TiO_2 and TiO_2 -FG shown IV isotherms, with less nitrogen adsorb quantity, these findings suggest limited surface area and the presence of mesoporous [226, 227]. The substantial specific surface area and the presence of numerous ultra-microspores in the HCP- TiO_2 -FG composite have prompted us to explore its gas adsorption capabilities [228, 229]. Remarkably, HCP- TiO_2 -FG exhibits CO_2 uptake, impressive 12.87% at 1 bar and 273.15 K , to contextualization these findings comparative analysis with various porous photocatalysts reported under analogues condition, as shown in Fig. 8e, f.

The integration of a semiconductor along with any photosensitizer or organic sacrificial reagent (Fig. 9a, b) shows

the production CO_2 conversion products within a 5 h photocatalytic reaction, facilitated under visible-light condition ($\lambda = 420\text{ nm}$). Notably, this processes yielded the primary gases CO and CH_4 , generated through $2e^-$ and $8e^-$ reduction processes [221]. The porous HCP- TiO_2 -FG catalyst exhibited a notable average conversion efficiency at rate R_e of $264\text{ }\mu\text{mol g}^{-1}\text{ h}^{-1}$. Additionally, CH_4 and CO rates are $27.6\text{ }\mu\text{mol g}^{-1}\text{ h}^{-1}$ and $21.63\text{ }\mu\text{mol g}^{-1}\text{ h}^{-1}$. Figure 9c shows as HCP- TiO_2 -FG material displayed a remarkable 83.7% electron consumption selectivity for CH_4 production, while also effectively preventing H_2 evolution during the photocatalytic reaction. This underscores its high selectivity of CO_2 photoreduction and the undesired H_2O reduction. CO_2 conversion products were scarcely observed ($< 1\text{ }\mu\text{mol g}^{-1}\text{ h}^{-1}$) in the case of commercial TiO_2 (P25) and pure TiO_2 featuring reactive (001) facets. This was primarily attributed to their constrained light absorption in the visible spectrum, in Fig. 9d. The combination of TiO_2 with graphene, resulting in TiO_2 -G, and significantly enhanced CH_4 production (to $2.42\text{ }\mu\text{mol g}^{-1}\text{ h}^{-1}$) through the improvement of visible-light adsorption and electron transport properties [230–232]. Incorporating porous HCPs layers enriched the adsorption sites, leading to elevated CO_2 uptake and enhanced visible-light absorption [233]. Consequently, the creation of the well-structural HCP- TiO_2 -FG composite significantly elevated the rate of photocatalytic CO_2 reduction. To assess the effectiveness of charge separation, transparent amperometric I–T curves were recorded during exposure to visible light. As shown in Fig. 9e, the resulting materials demonstrate excellent photocurrent stability throughout light on–off cycles, aligning consistently with the photocatalytic assessments. Notably, the pure TiO_2 system displayed a minimal signal, HCP-FG exhibits a weak photocurrent response, while the HCP- TiO_2 -FG composites show better current intensity [234]. The route for charge carrier transfer and separation is typically contingent on the band gap of the photocatalyst [235]. HCP-FG exhibits its highest occupied molecular orbital (HOMO) and lowest unoccupied molecular orbital (LUMO) energy levels positioned at -5.34 eV and -3.00 eV versus vacuum level shown in Fig. 9d obtained by optical absorption. An overarching framework delineating the CO_2 conversion process over the HCP- TiO_2 -FG photocatalyst is hereby put forth in Fig. 9f, and when exposed to visible-light irradiation, HCP-FG plays a dual role as a CO_2 adsorbent and a photosensitizer. It directly absorbs photons, thereby instigating the transition from the highest occupied molecular orbital (HOMO) to lowest unoccupied molecular orbital (LUMO) [236, 237].

Another brief mechanism for CO_2 reduction process over $CuInSnS_4$ a single metal sulfides, the context of this study, in situ Fourier-transform infrared spectroscopy is employed to analyze and contrast the reaction intermediates present on the catalyst surface [238]. No discernible macroscopic

Table 2 Summary of utilizing graphene and its derivative for CO₂ capture [191]

Material	Preparation method	Description precursor	Media	Physical properties	Chemical properties	Performance	References
Graphene	Thermal conversion	Nanodiamonds	1650 °C helium atmosphere	8–10 graphene layers, surface area: 280–1013 m ² /g	–	CO ₂ adsorption: 10–38 wt% (<i>P</i> = 1 atm, <i>T</i> = 195 K)	[192]
	Thermal exfoliation	Graphite flake	1050 °C Argon atmosphere	3–4 graphene layer, surface area: 639–1550 m ² /g	–	CO ₂ adsorption: 21–34 wt% (<i>P</i> = 1 atm, <i>T</i> = 195 K)	[192]
	Carbonization activation	Wood residue	KOH	Clear material voile like structure, surface area: 750–1735 m ² /g	FT-IR peaks: O–H, sp ³ and sp ² CH, C=C, C–OH	Highest CO ₂ adsorption capacity 12.68 mmol/g, (<i>P</i> = 10 bar, <i>T</i> = 293 K)	[193]
Graphene nanosheets	Modified hummer's method + ultrasonic dispersion	Graphite flake	H ₂ SO ₄ KmnO ₄ K ₂ FeO ₄	Microspores, surface area: 284–964 m ² /g	–	1.14 mmol/g	[194]
		Solid wastes	H ₂ SO ₄ KmnO ₄ K ₂ FeO ₄	Closely packed layer, microspores, surface area: 284–964 m ² /g	FT-IR peaks: C=O, aromatic C=C Carboxyl and epoxy C–O, NH ₂ , N–H, C–H	1.27–4.62 mmol/g	[194]
	Hummer's method	Graphite	H ₂ SO ₄ KmnO ₄	Microspores, surface area: 284–964 m ² /g	–	1.08 mmol/g	[194]
	Thermal oxidative reduction	Graphite	NaNO ₃ H ₂ SO ₄ H ₃ PO ₄ KmnO ₄	Wrinkled and corrugated structure, surface area: 94–484 m ² /g	–	2.89 mmol/g (<i>P</i> = 1 bar, <i>T</i> = 0 °C)	[195]
Graphene Nanoplates	Vacuum-assisted thermal reduction	Graphite flakes	CH ₃ COOH NaNO ₃ H ₂ SO ₄ KmnO ₄ , 150–400 °C	Microspores, surface area: 151–324 m ² /g, larger interlayer spacing and higher interior void volume	–	Highest CO ₂ capture capacity: 248 wt% (<i>P</i> = 30 bar, <i>T</i> = 25 °C)	[196]
Graphene oxide	Improved tour's method	Graphite flakes	H ₂ SO ₄ H ₃ PO ₄ KmnO ₄	Agglomerates of graphene sheets, surface area: 9.08 m ² /g	FT-IR peaks: OH, C=O, C=C, C–O, $\frac{I_{\text{D}}}{I_{\text{G}}}$: 1.07	1.1 mmol/g (<i>P</i> = 1 bar, <i>T</i> = 30 °C)	[197]
Reduced graphene oxide	Reduction-induced self-assembly	Graphene oxide	Ascorbic acid (AsA)	In homogenous distribution of larger macroscopic pores and a more homogenous distribution of smaller pores, surface area: 60–328 m ² /g	–	2.1 mmol/g (<i>P</i> = 1 atm, <i>T</i> = 25 °C)	[198]

Table 3 A summary of the designing of graphene-based photocatalyst for CO₂ reduction [199]

Photocatalyst	Catalyst synthetic protocol	Light source	Experimental condition for CO ₂ reduction	Product formed	Photocatalytic activity	References
GO	Hummer method + irradiation with solar & UV light	500W Xe lamp, stimulated sunlight; 4.5 h irradiation	CO ₂ (100 mL min ⁻¹)	CO (Sunlight irradiation)	1.23 μmol g ⁻¹ h ⁻¹	[200]
C ₅₄ PbBr ₆ /O/doped-rGO	Surfactant-mediated anti-solvent precipitation	300W Xe lamp	Ethyl acetate (5 mL)/DI H ₂ O (5 μL)	CO	11.4 μmol g ⁻¹ h ⁻¹	[201]
In ₂ O ₃ /O/doped-rGO	Sol-gel	250W Hg vapor lamp	NaOH (2 M)/CO ₂	CH ₄	953.72 μmol g ⁻¹ h ⁻¹	[202]
TiO ₂ /N/doped-rGO	Urea assisted hydrothermal	400 W Xe lamp	CO ₂ /H ₂ O (16 mL min ⁻¹)	CO	356.5 μmol g ⁻¹ h ⁻¹	[203]
CdS/N/doped-rGO	Chemical vapor deposition	300W Xe lamp	CO ₂ /H ₂ O	CO and CH ₄	CO(2.59) and CH ₄ (0.33) μmol g ⁻¹ h ⁻¹	[204]
Pt/Reduced Titania/N doped GO	Hydrothermal + photo deposition	100W Xe lamp	CO ₂ /H ₂ O (40 mL min ⁻¹)	CH ₄	252 nmol g ⁻¹	[205]
WSe ₂ /graphene/TiO ₂	Ultrasonic techniques	500W Xe lamp; 48 h reaction	Sacrificial reagent: H ₂ O + Na ₂ SO ₃	CH ₃ OH	6.3262 μmol g ⁻¹ h ⁻¹	[206]
ZnO/rGO	One-step hydrothermal	300W Xe lamp	1 M NaOH/CO ₂	CH ₃ OH	263.17 μmol g ⁻¹	[207]
TiO ₂ /rGO	Sonothermal-hydrothermal	8W UV lamp	ACN mixture (4:16 v/v)/TEOA	CH ₃ OH	2.33 mmol g ⁻¹ h ⁻¹	[208]
Graphene/g-C ₃ N ₄	Ultrasonic assisted + surface charge modification	15W daylight lamp; 10 h light irradiation	CO ₂ (5 mL min ⁻¹)/H ₂ O	CH ₄	13.93 μmol g ⁻¹	[209]
Porous g-C ₃ N ₄ /graphene oxide	Hydrothermal co-assembly	500W Xe lamp; 6 h irradiation	MO solution used	CO	23 mmol g ⁻¹	[210]
rGO/pg-C ₃ N ₄	Ultrasonic assisted + surface charge modification	15W daylight lamp; 10 h light irradiation	CO ₂ (5 mL min ⁻¹)/H ₂ O	CH ₄	13.93 μmol g ⁻¹	[211]
SiC/rGO	In-situ carbon templating	300W arc lamp; 4 h irradiation	CO ₂ /H ₂ O (100 μL)	CH ₄	58.17 μmol g ⁻¹ h ⁻¹	[212]
ZnV ₂ O ₆ /rGO	One-pot solvothermal	35W HID Xe lamp; 10 h irradiation	100 mL H ₂ O + 0.1 M NaOH; CO ₂ 20 (mL/min)	CH ₃ OH, CH ₃ COOH and HCOOH	CH ₃ OH(5154), CH ₃ COOH(385.44 μmol g ⁻¹), HCOOH(1942.41)	[213]
CuCaAg ₂ Se/TiO ₂ /GO	Muffled-assisted hydrothermal + pechini method	500W metal halide lamp; 48 h irradiation	Sacrificial scavenger: Na ₂ SO ₄ /50 mL DI water + NaHCO ₃ (0.04 M)	CH ₃ OH	Visible light: 12.68%, UV light: 16.84%	[214]
LaYAgO ₄ /TiO ₂ /GO	Hydrothermal	500W metal halide lamp; 48 h irradiation	Carbonated H ₂ O (50 mL)	CH ₃ OH	Visible light: 1758.4, UV light: 1945.9 mmol g ⁻¹	[215]

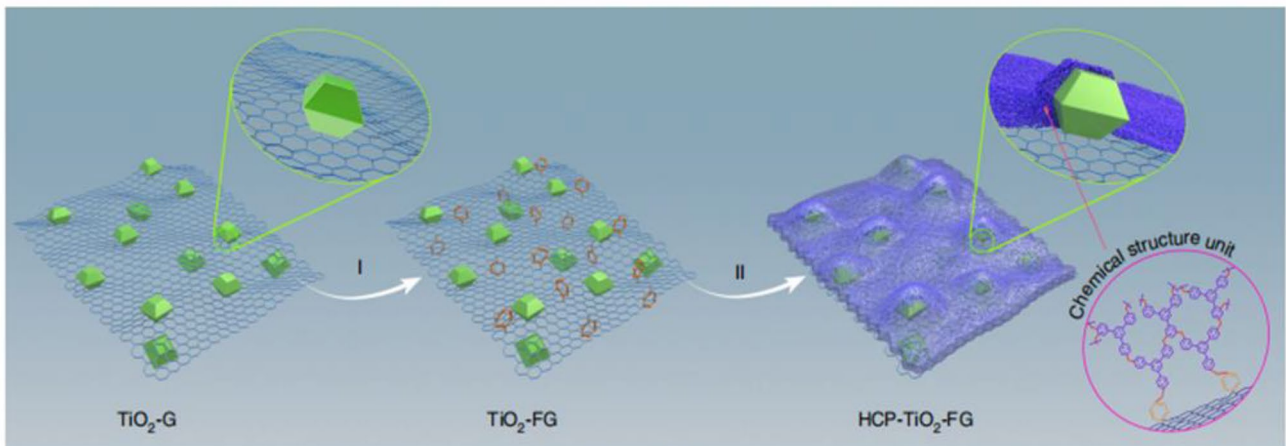


Fig. 7 (I) Enhancing the functionalization of $\text{TiO}_2\text{-G}$ through the formation of Diazonium salts. (II) Merging $\text{TiO}_2\text{-FG}$ with syn-PhPh_3 via solvent knitting technique. Upper right corner provide the detailed sectional view of the $\text{HCP-TiO}_2\text{-FG}$ composite [221]

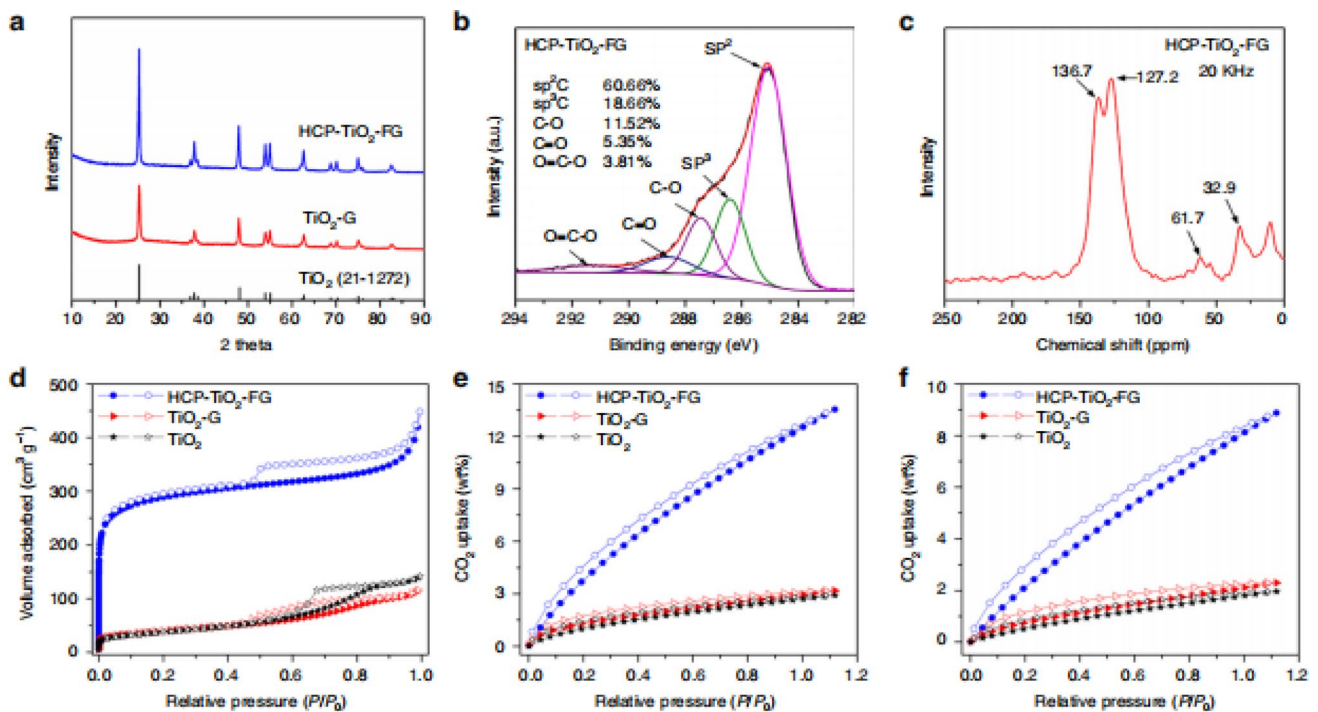


Fig. 8 Chemical composition, porous characteristics, and CO_2 adsorption capacity of different photocatalyst. **a** XRD image, **b** C^1 sketch $\text{HCP-TiO}_2\text{-FG}$, **c** C^{13} (CP/MAS), **d** N_2 adsorption at 77.3 K,

and **e, f** volumetric CO_2 adsorption and desorption at 273.15 K and at 298.15 K for 1 bar [221]

infrared absorption peaks corresponding to reaction intermediate are observed on Cu_2S SnS_2 even in the presence of light irradiation. This absence may be attributed to their limited chemical interaction with CO_2 [239]. Conversely, In_2S_3 exhibits a pronounced activation effect on CO_2 adsorption at the surface when subjected to light irradiation [240] in Fig. 10a. Even in the absence of light, CO_2 chemisorbs onto

In_2S_3 evident from the 1150 cm^{-1} IR peak denoting an O–S–stretching vibration [241], sufficient oxygen–sulfur bonding. The oxygen atom of CO_2 is chemically linked to the sulfur atom of In_2S_3 [242]. Under light exposure, specific infrared peaks on the catalyst surface are detected. 1225 cm^{-1} peak corresponding to bidentate bicarbonates vibrations, while the 1412 cm^{-1} peaks signifies monodentate bicarbonates

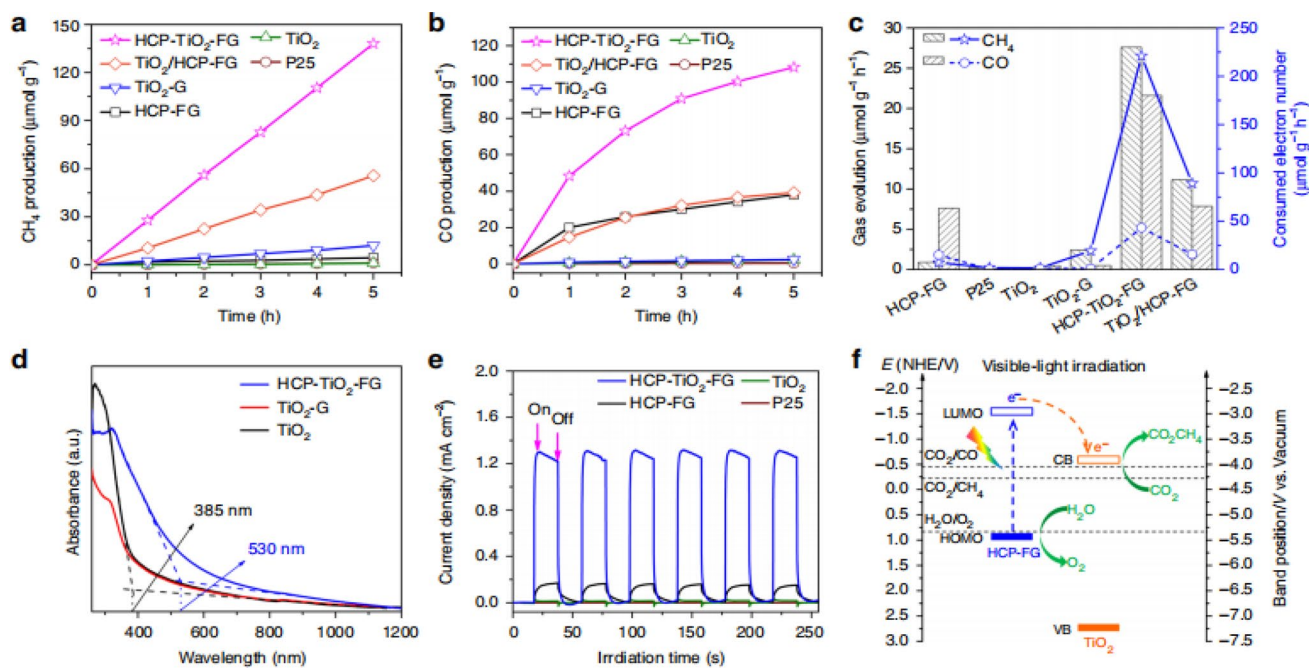


Fig. 9 The photoreduction of CO₂, optical and photoelectrical characteristics, and the intricacies of the charge transfer pathways all contribute to the assessment of the photocatalytic efficiency, specifically: **a** CH₄ and **b** CO in the context of photocatalytic CO₂ reduction, **c**

average conversion efficiency rate of CH₄ and CO, **d** UV absorption of catalyst, **e** amperometric I-T curve of sample, and **f** suggested mechanism of charge separation and transfer in the composite photocatalyst HCP-TiO₂-FG [221]

vibration [243]. Of particular significance, the 1610 cm⁻¹ peak is associated with the *COOH group, a critical intermediate in the CO₂ reduction to CO process. Remarkably, the polymetallic sulfide CuInSnS₄ displays robust CO₂ chemisorption and substantial H₂O physisorption (Fig. 10b).

The CO₂ adsorption configuration on CuInSnS₄ is pivotal in determining its outstanding CO₂ photoreduction activity and selectivity. To investigate the CO₂ conversion pathways on the CuInSnS₄ photocatalyst surface, DFT calculation were conducted, as shown in Fig. 11.

The adsorption arrangement of CuInSnS₄ is illustrated for each for each incremental step, encompassing CO₂ adsorption through CH₄ generation. Various intermediate states, including CO₂*, COOH, CHO*, CH₂O*, and CH₃* and their corresponding C atom are depicted which consistently maintain strong bonds with electron-deficient sulfur atoms on the (111) plane of the CuInSnS₄ nano-signal crystal.

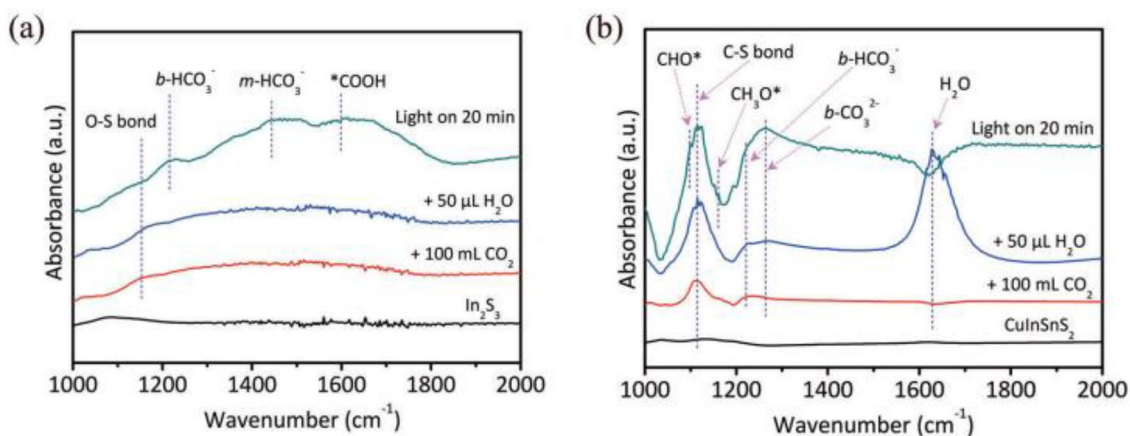
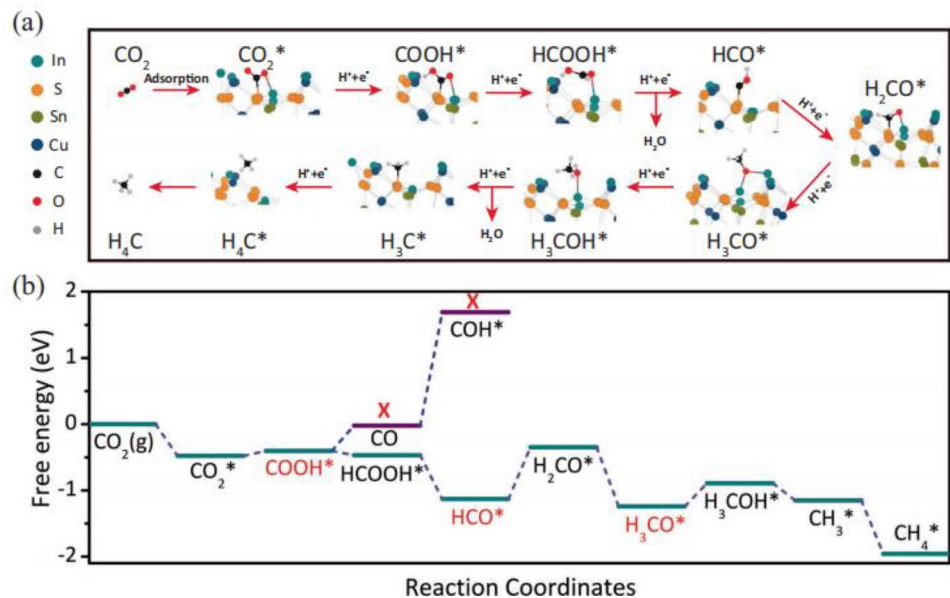


Fig. 10 In-situ FT-IR spectra for adsorbed CO₂: **a** In₂S₃ and **b** CuInSnS₄ [238]

Fig. 11 **a** Calculate adsorption configuration of CO_2 & reactive on CuInSnS_4 , and **b** Gibbs free energy of CO_2 to CH_4 [238]



8 Advantages of using carbon materials for CO_2 reduction

Using carbon materials in photocatalytic reaction has advantages like providing more spaces for reactions, making CO_2 easier to work with, separation of charges and absorbing more light energy for better performance. Materials made from carbon, like graphene oxide, graphene, carbon nanotubes (CNTs), and $g\text{-C}_3\text{N}_4$, offer an expanded surface area of the catalyst, when they are combined [244]. $g\text{-C}_3\text{N}_4$ has many imperfections on its surface, because it contains hydrogen atoms and has an abundance of electrons. These imperfections make it useful for catalytic reactions as they help electrons move around more easily on the surface of catalyst. Yang et al. created nanosheets made of NiAl-layered double hydroxide (NALDH). They then joined these nanosheets with $g\text{-C}_3\text{N}_4$ nanosheets and observed a very closed connection between the two nanosheets, forming a strong heterojunction [245, 246]. Additionally, they include graphene aerogels, which played a role in extending the structure into network-like structure. In this research, they used both graphene nanosheets as well as aerogels to enhance the performance of the photocatalyst. Creating these extremely close connections between sheets reduced the distance for the conveyance of electric charges and also gave plenty of active sites for chemical reaction to occur. Using N_2 adsorption–desorption measurements, a significant enhancement in the specific surface area and pore volume was determined over a broad range, as shown in Fig. 12a [247]. In recent work by Chen et al. combined porous carbon nanofiber with added nitrogen with the mixture of nickel and molybdenum phosphide (Mo/Ni-PS@PAN), they used a method involving phosphatization

to make the catalyst particular larger, increasing their size from 20 to 50 nm. They conducted carbonization to further enlarge the size. When nanoparticles of MoP were mixed with evenly spread-out nickel atoms, it produced a material known as NiMoP@NCPF , through the process of carbonization the size expanded from 50 to 100 nm, as shown in Fig. 12b, c. The porous structure of the material they obtained played a pivotal role in enhancing CO_2 adsorption while carrying out the photocatalytic reduction reaction as indicated in Fig. 12d [248].

Apart from the characteristic of pore structures, the way gases interact with the surface is also vital for CO_2 adsorption. Therefore, when we modify the surface of carbon materials, we can make CO_2 molecules more polar and thus enhance their adsorption. This is achieved by incorporating the fundamental functional group within the carbon framework [249–251]. Various forms of carbon materials have been utilized as support materials for the photoreduction of CO_2 . Carbon-based materials hold tremendous promise for their high efficiency in CO_2 adsorption to their adjustable structure and ample surface area [252]. As $g\text{-C}_3\text{N}_4$, it can have a substantial surface area. In certain instances, graphene materials can be modified by adding protons, utilizing substances that protonate to boost area of interest. In recent research, Wu et al. conducted innovative research where they used $g\text{-C}_3\text{N}_4$ as a template. They created layer of $g\text{-C}_3\text{N}_4$ and introduced a combination of Ni/Co metal into the empty spaces within $g\text{-C}_3\text{N}_4$ using phosphoric acid [253–255]. With the addition of different amounts of metal dopants, it caused a transformation in the microstructure leading to the formation of $g\text{-C}_3\text{N}_4\text{-Ni-Co}$ with various sizes, as shown in Fig. 13a–c. And by adding bimetallic dopant will create more holes in $g\text{-C}_3\text{N}_4$ which increase the nitrogen vacancies [256]. Figure 13d shows the

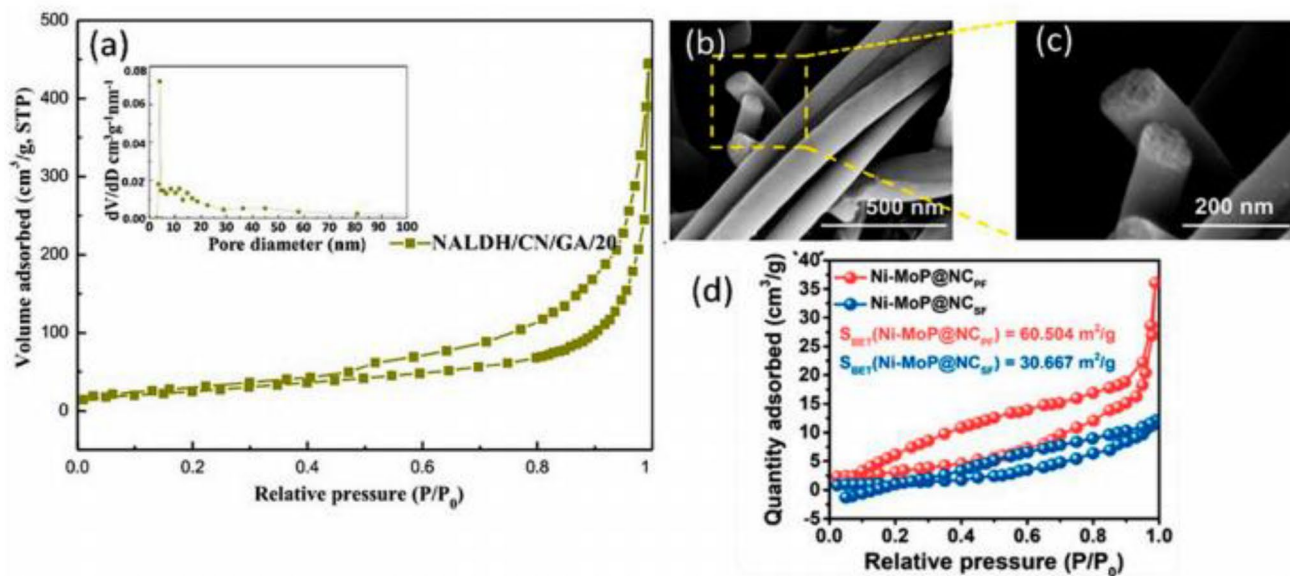


Fig. 12 **a** N_2 adsorption and desorption curves and the accompanying image depicting pore size spread image of NALDH. Reproduced with the permission from reference [247]. **b**, **c** SEM image of NiMoP@

NCPF, and **d** BET (Brunauer–Emmett–Teller) of NiMoP@NCPF and NiMoP@NCSF [248]

catalyst activity at different proportions and the by-product is formed is CO, the porous structure provides numerous spots and a broad catalytic surface area, speeding up the reaction. As a result, this significantly boost the CO production rate to 13.51 mmol/g/h, which is surpassing the achieved value by a factor 3.9 times, with g- C_3N_4 , as shown in Fig. 13e [257].

Numerous research articles have been extensively explored the field of CO_2 photoreduction, with semiconductor like TiO_2 emerging as the promising candidates for achieving reliable results. Despite notable achievements in this area, several challenges persist in the development of semiconductor photocatalyst, including low thermal and chemical stability, and reduced efficiency under specific conditions. In contrast, polymeric materials exhibit range of appealing characteristics, including cost-effectiveness, low toxicity, widespread availability, and light weight nature, ease of synthesis and use, and excellent flexibility [258, 259]. g- C_3N_4 stands out as an appealing polymeric photocatalyst, demonstrating superior performance even without the need for need metal composites of noble metal. In polymeric materials, the production of (e^-) and (h^+) pairs occurs more rapidly compared to semiconductor photocatalyst like g- C_3N_4 , primarily due to the presence of piled π bonds [260–263]. These accumulated π bonds within polymers facilitate instant charge transfer processes, as they were well candidates for catalyzing the CO_2 photocatalytic reduction [260, 264–267]. The role of

these stacked π bonds in CO_2 photoreduction is significant, although research in this area for π conjugated materials are still in its nascent stages. These stacked π bonds can play a pivotal role in the photoreduction of CO_2 ; however, research on π conjugated materials is still in nascent stages [258].

Intensified research into polymeric materials derived from carbon holds greater promise for enhancing the photocatalytic reduction of CO_2 when compared to current semiconductor photocatalyst. While these promising materials have shown favorable outcomes, further adjustments and the fine-tuning of band gaps are essential to achieve optimal results. It is crucial to consider both materials design and reaction methodology in this context. However, equally significant is evaluating the overall performance and sustainability of the entire energy generation and conversion process. With the aim of producing environmentally friendly fuels and mitigating the greenhouse effect in the future, it necessitates a more through and expansive investigation. This entails employing advanced tools and conducting detailed studies to gain a deeper understanding of these reaction [267–270].

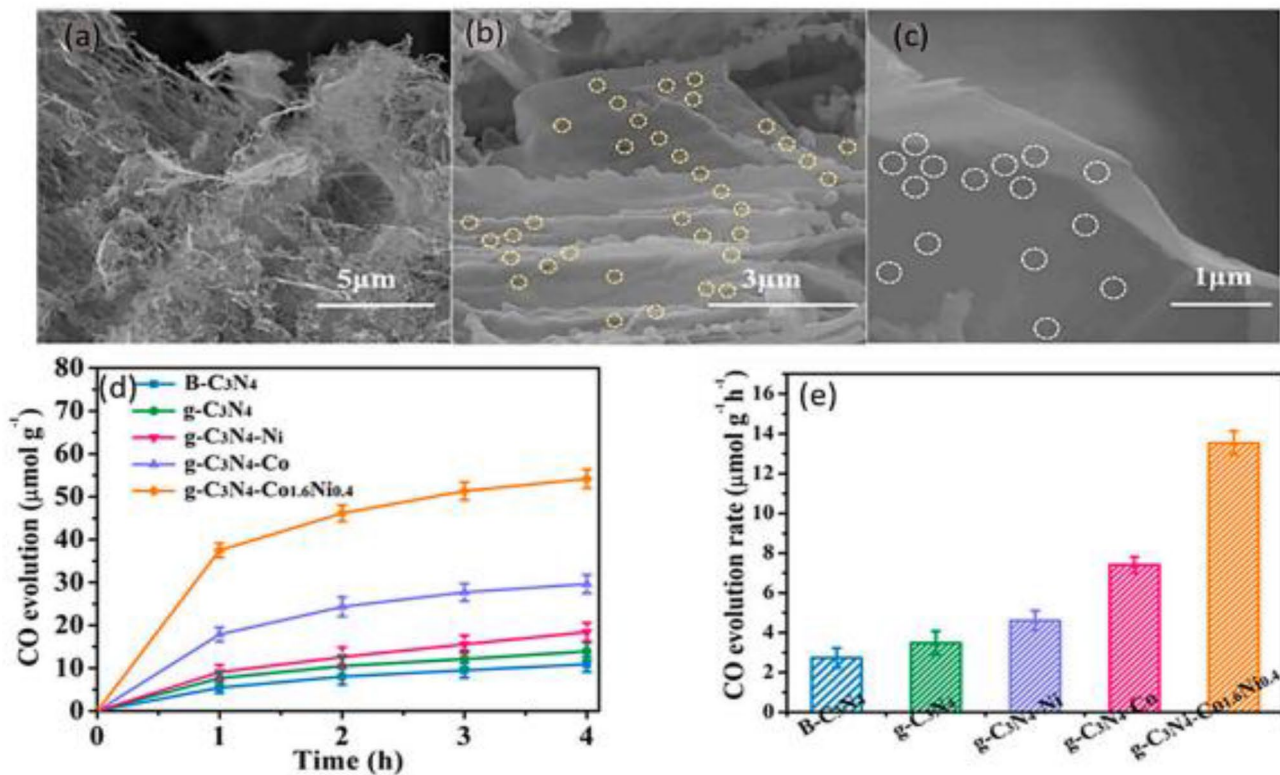


Fig. 13 a–c SEM visual representation of g-C₃N₄-Co_{1.6}Ni_{0.4} in various sizes, d CO generation time, and e CO production rate g-C₃N₄-Co_x-Ni_y [257]

9 Conclusion

In a global context increasingly oriented toward sustainable solutions, photocatalytic carbon dioxide photoreduction emerges as a pioneering innovation, presenting a promising avenue for addressing carbon emissions. By leveraging the transformative potential of light to convert carbon dioxide into valuable resources, this approach not only tackles environmental challenges but also unveils a spectrum of possibilities for cleaner energy and greener technologies. This comprehensive review primarily centers on elucidating the factors influencing product outcomes in CO₂ photoreduction.

CO₂ photoreduction, while holding promise as a sustainable approach for mitigating carbon emissions, confronts several challenges. The primary hurdle lies in the inherently low efficiency of the photoreduction process due to the limited absorption of solar radiation by CO₂ and the competitive reduction of protons to hydrogen. Furthermore, a significant challenge is the selectivity toward desired products, often resulting in the generation of undesired by-products. Product distribution forms the basis for tailoring catalyst yield of desired products, emphasizing the necessity of achieving a delicate equilibrium between product selectivity and overall process efficiency. Thermodynamic considerations, such as

redox potential and Gibbs free energy, offer insights into the energy requirements and feasibility of the process, predicting electron pathways and routes for optimal conditions conducive to efficient CO₂ reduction. Additionally, the adsorption and CO₂ activation properties eliminate product oxidation, maximizing efficiency. This implies that a purposefully engineered semiconductor with an enhanced adsorption ratio facilitates reaction kinetics.

Optimizing the compositional balance between these factors, although challenging, is essential for achieving high efficiency in CO₂ photoreduction, necessitating further modifications. To ascertain production yield, differentiation between derivation from CO₂ and impurities is imperative, achievable through isotope labeling in nano-scale probes.

To address the challenges involved in engineering of photocatalytic materials with enhanced properties' development of innovative reactor system is crucial. Perspective solutions involve the engineering of photocatalytic materials with enhanced light absorption properties and tailored catalytic sites for improved selectivity. Integration of tandem catalysis, wherein multiple catalytic processes are sequentially coupled, may further enhance overall efficiency. Future strategies should focus on the exploration of novel materials, such as semiconductor nanomaterial and molecular catalysts, and

the implementation of advanced computational approaches to guide catalyst design. Concurrently, a thorough investigation into photostability is imperative. The development of a robust and stable photocatalytic system capable of sustained operation under diverse conditions remains a critical objective. Additionally, efforts toward understanding the fundamental mechanistic aspects of CO₂ photoreduction will be pivotal for optimizing and scaling up this technology to contribute substantively to carbon management and sustainable energy systems.

Declarations

Conflict of interest The authors declare that there is no conflict of interest regarding the publication of this paper.

References

1. J. Ma, N. Sun, X. Zhang, N. Zhao, F. Xiao, W. Wei, Y. Sun, A short review of catalysis for CO₂ conversion. *Catal. Today* **148**, 221–231 (2009)
2. Z. Sun, J. Dong, C. Chen, S. Zhang, Y. Zhu, Photocatalytic and electrocatalytic CO₂ conversion: from fundamental principles to design of catalysts. *J. Chem. Technol. Biotechnol.* **96**, 1161–1175 (2021)
3. S. Zhang, Q. Fan, R. Xia, T.J. Meyer, CO₂ reduction: from homogeneous to heterogeneous electrocatalysis. *Acc. Chem. Res.* **53**, 255–264 (2020)
4. X. Li, J. Wen, J. Low, Y. Fang, J. Yu, Design and fabrication of semiconductor photocatalyst for photocatalytic reduction of CO₂ to solar fuel. *Sci. China Mater.* **57**, 70–100 (2014)
5. A.J. Bard, M.A. Fox, Artificial photosynthesis: solar splitting of water to hydrogen and oxygen. *Acc. Chem. Res.* **28**, 141–145 (1995)
6. M.G. Walter, E.L. Warren, J.R. McKone, S.W. Boettcher, Q. Mi, E.A. Santori, N.S. Lewis, Solar water splitting cells. *Chem. Rev.* **110**, 6446–6473 (2010)
7. X. Chen, S. Shen, L. Guo, S.S. Mao, Semiconductor-based photocatalytic hydrogen generation. *Chem. Rev.* **110**, 6503–6570 (2010)
8. D. Cheng, H.H. Ngo, W. Guo, S.W. Chang, D.D. Nguyen, Y. Liu, X. Zhang, X. Shan, Y. Liu, Contribution of antibiotics to the fate of antibiotic resistance genes in anaerobic treatment processes of swine wastewater: a review. *Biores. Technol.* **299**, 122654 (2020)
9. S. Dahl, I. Chorkendorff, Towards practical implementation. *Nat. Mater.* **11**, 100–101 (2012)
10. V.N.H. Nguyen, T.H. Nguyen, M.S. Lee, Review on the comparison of the chemical reactivity of Cyanex 272, Cyanex 301 and Cyanex 302 for their application to metal separation from acid media. *Metals* **10**, 1105 (2020)
11. S. Lingampalli, M.M. Ayyub, C. Rao, Recent progress in the photocatalytic reduction of carbon dioxide. *ACS Omega* **2**, 2740–2748 (2017)
12. S. Sato, T. Arai, T. Morikawa, K. Uemura, T.M. Suzuki, H. Tanaka, T. Kajino, Selective CO₂ conversion to formate conjugated with H₂O oxidation utilizing semiconductor/complex hybrid photocatalysts. *J. Am. Chem. Soc.* **133**, 15240–15243 (2011)
13. S.-Y. Liu, A. Zada, X. Yu, F. Liu, G. Jin, NiFe₂O₄/g-C₃N₄ heterostructure with an enhanced ability for photocatalytic degradation of tetracycline hydrochloride and antibacterial performance. *Chemosphere* **307**, 135717 (2022)
14. Z. Liao, Y. Wu, S. Cao, S. Zhao, X. Yan, S. Yuan, K. Dong, J. Qin, C. Ou, J. Zhu, Facile engineering of PES ultrafiltration membranes using polyoxometalates for enhanced filtration and antifouling performance. *Sep. Purif. Technol.* **308**, 122911 (2023)
15. A. Kudo, Y. Miseki, Heterogeneous photocatalyst materials for water splitting. *Chem. Soc. Rev.* **38**, 253–278 (2009)
16. K. Maeda, K. Domen, New non-oxide photocatalysts designed for overall water splitting under visible light. *J. Phys. Chem. C* **111**, 7851–7861 (2007)
17. P. Dhull, A. Sudhaik, V. Sharma, P. Raizada, V. Hasija, N. Gupta, T. Ahamad, V.-H. Nguyen, A. Kim, M. Shokouhimehr, An overview on InVO₄-based photocatalysts: electronic properties, synthesis, enhancement strategies, and photocatalytic applications. *Mol. Catal.* **539**, 113013 (2023)
18. N. Shehzad, M. Tahir, K. Johari, T. Murugesan, M. Hussain, Improved interfacial bonding of graphene-TiO₂ with enhanced photocatalytic reduction of CO₂ into solar fuel. *J. Environ. Chem. Eng.* **6**, 6947–6957 (2018)
19. L. Wei, C. Yu, Q. Zhang, H. Liu, Y. Wang, TiO₂-based heterojunction photocatalysts for photocatalytic reduction of CO₂ into solar fuels. *J. Mater. Chem. A* **6**, 22411–22436 (2018)
20. J. Cai, F. Shen, Z. Shi, Y. Lai, J. Sun, Nanostructured TiO₂ for light-driven CO₂ conversion into solar fuels. *APL Mater.* **8**, 1 (2020)
21. X. Yu, V.V. Ordonsky, A.Y. Khodakov, Selective deposition of cobalt and copper oxides on BiVO₄ facets for enhancement of CO₂ photocatalytic reduction to hydrocarbons. *ChemCatChem* **12**, 740–749 (2020)
22. X. Wang, Y. Wang, M. Gao, J. Shen, X. Pu, Z. Zhang, H. Lin, X. Wang, BiVO₄/Bi₄Ti₃O₁₂ heterojunction enabling efficient photocatalytic reduction of CO₂ with H₂O to CH₃OH and CO. *Appl. Catal. B* **270**, 118876 (2020)
23. X. Li, D. Wei, L. Ye, Z. Li, Fabrication of Cu₂O-RGO/BiVO₄ nanocomposite for simultaneous photocatalytic CO₂ reduction and benzyl alcohol oxidation under visible light. *Inorg. Chem. Commun.* **104**, 171–177 (2019)
24. B. Han, X. Ou, Z. Deng, Y. Song, C. Tian, H. Deng, Y.J. Xu, Z. Lin, Nickel metal–organic framework monolayers for photoreduction of diluted CO₂: metal-node-dependent activity and selectivity. *Angew. Chem. Int. Ed.* **57**, 16811–16815 (2018)
25. K. Song, X. Qiu, B. Han, S. Liang, Z. Lin, Efficient upcycling electroplating sludge and waste PET into Ni-MOF nanocrystals for the effective photoreduction of CO₂. *Environ. Sci. Nano* **8**, 390–398 (2021)
26. H.-N. Wang, H.-X. Sun, Y.-M. Fu, X. Meng, Y.-H. Zou, Y.-O. He, R.-G. Yang, Varied proton conductivity and photoreduction CO₂ performance of isostructural heterometallic cluster based metal–organic frameworks. *Inorgan. Chem. Front.* **8**, 4062–4071 (2021)
27. M. Que, Y. Zhao, Y. Yang, L. Pan, W. Lei, W. Cai, H. Yuan, J. Chen, G. Zhu, Anchoring of formamidinium lead bromide quantum dots on Ti₃C₂ nanosheets for efficient photocatalytic reduction of CO₂. *ACS Appl. Mater. Interfaces* **13**, 6180–6187 (2021)
28. K. Ren, S. Yue, C. Li, Z. Fang, K.A. Gasem, J. Leszczynski, S. Qu, Z. Wang, M. Fan, Metal halide perovskites for photocatalysis applications. *J. Mater. Chem. A* **10**, 407–429 (2022)
29. S. Park, S. Choi, S. Kim, K.T. Nam, Metal halide perovskites for solar fuel production and photoreactions. *J. Phys. Chem. Lett.* **12**, 8292–8301 (2021)
30. Y. Cui, P. Ge, M. Chen, L. Xu, Research progress in semiconductor materials with application in the photocatalytic reduction of CO₂. *Catalysts* **12**, 372 (2022)
31. R. Sharma, M. Khanuja, S.N. Sharma, O.P. Sinha, Reduced band gap & charge recombination rate in Se doped α -Bi₂O₃ leads to enhanced photoelectrochemical and photocatalytic performance:

- theoretical and experimental insight. *Int. J. hydrog. Energy* **42**, 20638–20648 (2017)
32. J. Xiong, M. Zhang, M. Lu, K. Zhao, C. Han, G. Cheng, Z. Wen, Achieving simultaneous Cu particles anchoring in mesoporous TiO₂ nanofabrication for enhancing photo-catalytic CO₂ reduction through rapid charge separation. *Chin. Chem. Lett.* **33**, 1313–1316 (2022)
 33. H. Yu, J. Huang, L. Jiang, X. Yuan, K. Yi, W. Zhang, J. Zhang, H. Chen, Steering photo-excitons towards active sites: intensified substrates affinity and spatial charge separation for photocatalytic molecular oxygen activation and pollutant removal. *Chem. Eng. J.* **408**, 127334 (2021)
 34. F. Khodabandelo, S. Shahsavari, B. Nayebi, K.P. Niavol, B. Nayebi, R.S. Varma, J.H. Cha, H.W. Jang, D. Kim, M. Shokouhimehr, Applications of nanostructured semiconductor photocatalysts for the decontamination of assorted pollutants from wastewater. *Inorgan. Chem. Commun.* **2023**, 111357 (2023)
 35. M. Zhu, X. Zhang, H. Feng, J. Dai, J. Li, Q. Che, Q. Gu, T. Zhu, D. Li, Penicisulfuranols A–F, alkaloids from the mangrove endophytic fungus *Penicillium janthinellum* HDN13-309. *J. Nat. Prod.* **80**, 71–75 (2017)
 36. H. Maleki-Ghaleh, M. Shakeri, Z. Dargahi, M. Kavanlouei, H.K. Garabagh, E. Moradpur-Tari, A. Yourdkhani, A. Fallah, A. Zarrabi, B. Koç, Characterization and optical properties of mechanochemically synthesized molybdenum-doped rutile nanoparticles and their electronic structure studies by density functional theory. *Mater. Today Chem.* **24**, 100820 (2022)
 37. N.U.M. Nor, E. Mazalan, C. Risko, M. Crocker, N.A.S. Amin, Unveiling the structural, electronic, and optical effects of carbon-doping on multi-layer anatase TiO₂ (1 0 1) and the impact on photocatalysis. *Appl. Surf. Sci.* **586**, 152641 (2022)
 38. C. Feng, Z. Chen, W. Li, F. Zhang, X. Li, L. Xu, M. Sun, First-principle calculation of the electronic structures and optical properties of the metallic and nonmetallic elements-doped ZnO on the basis of photocatalysis. *Physica B* **555**, 53–60 (2019)
 39. M. Kapilashrami, Y. Zhang, Y.-S. Liu, A. Hagfeldt, J. Guo, Probing the optical property and electronic structure of TiO₂ nanomaterials for renewable energy applications. *Chem. Rev.* **114**, 9662–9707 (2014)
 40. S. Xu, E.A. Carter, Theoretical insights into heterogeneous (photo) electrochemical CO₂ reduction. *Chem. Rev.* **119**, 6631–6669 (2018)
 41. H. Yang, F. Teng, W. Gu, Z. Liu, Y. Zhao, A. Zhang, Z. Liu, Y. Teng, A simple post-synthesis conversion approach to Zn(OH)F and the effects of fluorine and hydroxyl on the photodegradation properties of dye wastewater. *J. Hazard. Mater.* **333**, 250–258 (2017)
 42. Z. Zhang, L. Wang, W. Liu, Z. Yan, Y. Zhu, S. Zhou, S. Guan, Photogenerated-hole-induced rapid elimination of solid tumors by the supramolecular porphyrin photocatalyst. *Natl. Sci. Rev.* **8**, naa155 (2021)
 43. I. Okeke, C. Okeke, Molecular docking and analysis of in silico generated ligands against SARS-CoV-2 spike and replicase proteins (2022). <https://doi.org/10.21203/rs.3.rs-2069911/v1>.
 44. C.O.L. Mbuya, C.G. Okoye-Chine, K. Ramutsindela, L.L. Jewell, M. Scurrell, Microwave modification of iron supported on beta silicon carbide catalysts for Fischer–Tropsch synthesis. *React. Chem. Eng.* **7**, 1307–1314 (2022)
 45. R. Gandhi, A. Moses, S.S. Baral, Fundamental study of the photocatalytic reduction of CO₂: a short review of thermodynamics, kinetics and mechanisms. *Chem. Process. Eng.* **43**, 223–228 (2022)
 46. T. Mavrič, *Synthesis and characterization of metal/semiconductor nanocomposites for photocatalysis* (Univerza v Novi Gorici, Fakulteta za podiplomski študij, 2017)
 47. H. Liang, H. Zhang, P. Zhao, X. Zhao, H. Sun, Z. Geng, D. She, Synthesis of a novel three-dimensional porous carbon material and its highly selective Cr(VI) removal in wastewater. *J. Clean. Prod.* **306**, 127204 (2021)
 48. J.R. Bolton, Solar fuels: the production of energy-rich compounds by the photochemical conversion and storage of solar energy. *Science* **202**, 705–711 (1978)
 49. J.-M. Lehn, R. Ziessel, Photochemical generation of carbon monoxide and hydrogen by reduction of carbon dioxide and water under visible light irradiation. *Proc. Natl. Acad. Sci.* **79**, 701–704 (1982)
 50. X. Tan, Y. Jiang, Y. Chen, A. Tong, J. Li, Y. Sun, Roles of different components of complex inclusion in pitting of 321 stainless steel: induction effect of CaS and inhibition effect of TiN. *Corros. Sci.* **209**, 110692 (2022)
 51. G. Yasin, S. Ibraheem, S. Ali, M. Arif, S. Ibrahim, R. Iqbal, A. Kumar, M. Tabish, M. Mushtaq, A. Saad, Defects-engineered tailoring of tri-doped interlinked metal-free bifunctional catalyst with lower Gibbs free energy of OER/HER intermediates for overall water splitting. *Mater. Today Chem.* **23**, 100634 (2022)
 52. X. Li, J. Yu, M. Jaroniec, X. Chen, Cocatalysts for selective photoreduction of CO₂ into solar fuels. *Chem. Rev.* **119**, 3962–4179 (2019)
 53. K. Nakata, A. Fujishima, TiO₂ photocatalysis: design and applications. *J. Photochem. Photobiol. C* **13**, 169–189 (2012)
 54. A.L. Linsebigler, G. Lu, J.T. Yates Jr., Photocatalysis on TiO₂ surfaces: principles, mechanisms, and selected results. *Chem. Rev.* **95**, 735–758 (1995)
 55. A. Dhakshinamoorthy, S. Navalon, A. Corma, H. Garcia, Photocatalytic CO₂ reduction by TiO₂ and related titanium containing solids. *Energy Environ. Sci.* **5**, 9217–9233 (2012)
 56. V.P. Indrakanti, J.D. Kubicki, H.H. Schobert, Photoinduced activation of CO₂ on Ti-based heterogeneous catalysts: current state, chemical physics-based insights and outlook. *Energy Environ. Sci.* **2**, 745–758 (2009)
 57. T. Inoue, A. Fujishima, S. Konishi, K. Honda, Photoelectrocatalytic reduction of carbon dioxide in aqueous suspensions of semiconductor powders. *Nature* **277**, 637–638 (1979)
 58. J. Nunez, P. Jana, J.M. Coronado, D.P. Serrano, Effect of copper on the performance of ZnO and ZnO_{1-x}N_x oxides as CO₂ photoreduction catalysts. *Catal. Today* **209**, 21–27 (2013)
 59. G. Xi, S. Ouyang, J. Ye, General synthesis of hybrid TiO₂ mesoporous “French fries” toward improved photocatalytic conversion of CO₂ into hydrocarbon fuel: a case of TiO₂/ZnO. *Chem. A Eur. J.* **17**, 9057–9061 (2011)
 60. G. Guan, T. Kida, A. Yoshida, Reduction of carbon dioxide with water under concentrated sunlight using photocatalyst combined with Fe-based catalyst. *Appl. Catal. B* **41**, 387–396 (2003)
 61. G. Mahmodi, S. Sharifnia, F. Rahimpour, S. Hosseini, Photocatalytic conversion of CO₂ and CH₄ using ZnO coated mesh: effect of operational parameters and optimization. *Sol. Energy Mater. Sol. Cells* **111**, 31–40 (2013)
 62. H. Inoue, H. Moriwaki, K. Maeda, H. Yoneyama, Photoreduction of carbon dioxide using chalcogenide semiconductor microcrystals. *J. Photochem. Photobiol. A* **86**, 191–196 (1995)
 63. H. Fujiwara, H. Hosokawa, K. Murakoshi, Y. Wada, S. Yanagida, Surface characteristics of ZnS nanocrystallites relating to their photocatalysis for CO₂ reduction. *Langmuir* **14**, 5154–5159 (1998)

64. K. Kočí, M. Reli, O. Kozák, Z. Lacný, D. Plachá, P. Praus, L. Obalová, Influence of reactor geometry on the yield of CO₂ photocatalytic reduction. *Catal. Today* **176**, 212–214 (2011)
65. H. Zhou, J. Guo, P. Li, T. Fan, D. Zhang, J. Ye, Leaf-architected 3D hierarchical artificial photosynthetic system of perovskite titanates towards CO₂ photoreduction into hydrocarbon fuels. *Sci. Rep.* **3**, 1667 (2013)
66. B. Aurian-Blajeni, M. Halmann, J. Manassen, Photoreduction of carbon dioxide and water into formaldehyde and methanol on semiconductor materials. *Sol. Energy* **25**, 165–170 (1980)
67. D. Sui, X. Yin, H. Dong, S. Qin, J. Chen, W. Jiang, Photocatalytically reducing CO₂ to methyl formate in methanol over Ag loaded SrTiO₃ nanocrystal catalysts. *Catal. Lett.* **142**, 1202–1210 (2012)
68. W.-H. Lee, C.-H. Liao, M.-F. Tsai, C.-W. Huang, J.C. Wu, A novel twin reactor for CO₂ photoreduction to mimic artificial photosynthesis. *Appl. Catal. B* **132**, 445–451 (2013)
69. S. Yamamura, H. Kojima, J. Iyoda, W. Kawai, Formation of ethyl alcohol in the photocatalytic reduction of carbon dioxide by SiC and ZnSe/metal powders. *J. Electroanal. Chem. Interfacial Electrochem.* **225**, 287–290 (1987)
70. H. Li, Y. Lei, Y. Huang, Y. Fang, Y. Xu, L. Zhu, X. Li, Photocatalytic reduction of carbon dioxide to methanol by Cu₂O/SiC nanocrystallite under visible light irradiation. *J. Nat. Gas Chem.* **20**, 145–150 (2011)
71. T.-C. Yang, F.-C. Chang, C.-Y. Peng, H.P. Wang, Y.-L. Wei, Photocatalytic reduction of CO₂ with SiC recovered from silicon sludge wastes. *Environ. Technol.* **36**, 2987–2990 (2015)
72. Y. Li, W.-N. Wang, Z. Zhan, M.-H. Woo, C.-Y. Wu, P. Biswas, Photocatalytic reduction of CO₂ with H₂O on mesoporous silica supported Cu/TiO₂ catalysts. *Appl. Catal. B* **100**, 386–392 (2010)
73. I.-H. Tseng, W.-C. Chang, J.C. Wu, Photoreduction of CO₂ using sol-gel derived titania and titania-supported copper catalysts. *Appl. Catal. B* **37**, 37–48 (2002)
74. Y. Bessekhouad, D. Robert, J.-V. Weber, Photocatalytic activity of Cu₂O/TiO₂, Bi₂O₃/TiO₂ and ZnMn₂O₄/TiO₂ heterojunctions. *Catal. Today* **101**, 315–321 (2005)
75. D. Robert, Photosensitization of TiO₂ by MxOy and MxSy nanoparticles for heterogeneous photocatalysis applications. *Catal. Today* **122**, 20–26 (2007)
76. H. Fujiwara, H. Hosokawa, K. Murakoshi, Y. Wada, S. Yanagida, T. Okada, H. Kobayashi, Effect of surface structures on photocatalytic CO₂ reduction using quantized CdS nanocrystallites. *J. Phys. Chem. B* **101**, 8270–8278 (1997)
77. B.-J. Liu, T. Torimoto, H. Yoneyama, Photocatalytic reduction of CO₂ using surface-modified CdS photocatalysts in organic solvents. *J. Photochem. Photobiol. A* **113**, 93–97 (1998)
78. X. Li, J. Chen, H. Li, J. Li, Y. Xu, Y. Liu, J. Zhou, Photoreduction of CO₂ to methanol over Bi₂S₃/CdS photocatalyst under visible light irradiation. *J. Nat. Gas Chem.* **20**, 413–417 (2011)
79. P. Praus, O. Kozák, K. Kočí, A. Panáček, R. Dvorský, CdS nanoparticles deposited on montmorillonite: preparation, characterization and application for photoreduction of carbon dioxide. *J. Colloid Interface Sci.* **360**, 574–579 (2011)
80. Y.S. Chaudhary, T.W. Woolerton, C.S. Allen, J.H. Warner, E. Pierce, S.W. Ragsdale, F.A. Armstrong, Visible light-driven CO₂ reduction by enzyme coupled CdS nanocrystals. *Chem. Commun.* **48**, 58–60 (2012)
81. X. Li, H. Liu, D. Luo, J. Li, Y. Huang, H. Li, Y. Fang, Y. Xu, L. Zhu, Adsorption of CO₂ on heterostructure CdS (Bi₂S₃)/TiO₂ nanotube photocatalysts and their photocatalytic activities in the reduction of CO₂ to methanol under visible light irradiation. *Chem. Eng. J.* **180**, 151–158 (2012)
82. E.E. Barton, D.M. Rampulla, A.B. Bocarsly, Selective solar-driven reduction of CO₂ to methanol using a catalyzed p-GaP based photoelectrochemical cell. *J. Am. Chem. Soc.* **130**, 6342–6344 (2008)
83. K. Sekizawa, K. Maeda, K. Domen, K. Koike, O. Ishitani, Artificial Z-scheme constructed with a supramolecular metal complex and semiconductor for the photocatalytic reduction of CO₂. *J. Am. Chem. Soc.* **135**, 4596–4599 (2013)
84. M. Hara, J. Nunoshige, T. Takata, J.N. Kondo, K. Domen, Unusual enhancement of H₂ evolution by Ru on TaON photocatalyst under visible light irradiation. *Chem. Commun.* **2003**, 3000–3001 (2003)
85. E.S. Kim, N. Nishimura, G. Magesh, J.Y. Kim, J.-W. Jang, H. Jun, J. Kubota, K. Domen, J.S. Lee, Fabrication of CaFe₂O₄/TaON heterojunction photoanode for photoelectrochemical water oxidation. *J. Am. Chem. Soc.* **135**, 5375–5383 (2013)
86. K. Maeda, M. Higashi, D. Lu, R. Abe, K. Domen, Efficient nonsacrificial water splitting through two-step photoexcitation by visible light using a modified oxynitride as a hydrogen evolution photocatalyst. *J. Am. Chem. Soc.* **132**, 5858–5868 (2010)
87. J. Mao, T. Peng, X. Zhang, K. Li, L. Ye, L. Zan, Effect of graphitic carbon nitride microstructures on the activity and selectivity of photocatalytic CO₂ reduction under visible light. *Catal. Sci. Technol.* **3**, 1253–1260 (2013)
88. J. Yu, S. Wang, B. Cheng, Z. Lin, F. Huang, Noble metal-free Ni(OH) 2-gC₃N₄ composite photocatalyst with enhanced visible-light photocatalytic H₂-production activity. *Catal. Sci. Technol.* **3**, 1782–1789 (2013)
89. J. Zhang, X. Chen, K. Takanae, K. Maeda, K. Domen, J.D. Epping, X. Fu, M. Antonietti, X. Wang, Synthesis of a carbon nitride structure for visible-light catalysis by copolymerization. *Angew. Chem. Int. Ed.* **49**, 441–444 (2010)
90. A. Kudo, K. Ueda, H. Kato, I. Mikami, Photocatalytic O₂ evolution under visible light irradiation on BiVO₄ in aqueous AgNO₃ solution. *Catal. Lett.* **53**, 229–230 (1998)
91. A. Kudo, K. Omori, H. Kato, A novel aqueous process for preparation of crystal form-controlled and highly crystalline BiVO₄ powder from layered vanadates at room temperature and its photocatalytic and photophysical properties. *J. Am. Chem. Soc.* **121**, 11459–11467 (1999)
92. S. Tokunaga, H. Kato, A. Kudo, Selective preparation of monoclinic and tetragonal BiVO₄ with scheelite structure and their photocatalytic properties. *Chem. Mater.* **13**, 4624–4628 (2001)
93. H. Jiang, H. Dai, X. Meng, K. Ji, L. Zhang, J. Deng, Porous olive-like BiVO₄: alcohol-hydrothermal preparation and excellent visible-light-driven photocatalytic performance for the degradation of phenol. *Appl. Catal. B* **105**, 326–334 (2011)
94. H. Jiang, X. Meng, H. Dai, J. Deng, Y. Liu, L. Zhang, Z. Zhao, R. Zhang, High-performance porous spherical or octapod-like single-crystalline BiVO₄ photocatalysts for the removal of phenol and methylene blue under visible-light illumination. *J. Hazard. Mater.* **217**, 92–99 (2012)
95. W.-J. Chun, A. Ishikawa, H. Fujisawa, T. Takata, J.N. Kondo, M. Hara, M. Kawai, Y. Matsumoto, K. Domen, Conduction and valence band positions of Ta₂O₅, TaON, and Ta₃N₅ by UPS and electrochemical methods. *J. Phys. Chem. B* **107**, 1798–1803 (2003)
96. M. Higashi, K. Domen, R. Abe, Fabrication of efficient TaON and Ta₃N₅ photoanodes for water splitting under visible light irradiation. *Energy Environ. Sci.* **4**, 4138–4147 (2011)
97. Y. Li, T. Takata, D. Cha, K. Takanae, T. Minegishi, J. Kubota, K. Domen, Vertically aligned Ta₃N₅ nanorod arrays for solar-driven photoelectrochemical water splitting. *Adv. Mater.* **25**, 125–131 (2013)
98. S.S.K. Ma, T. Hisatomi, K. Maeda, Y. Moriya, K. Domen, Enhanced water oxidation on Ta₃N₅ photocatalysts by

- modification with alkaline metal salts. *J. Am. Chem. Soc.* **134**, 19993–19996 (2012)
99. X. Yang, C. Cao, L. Erickson, K. Hohn, R. Maghirang, K. Klabunde, Synthesis of visible-light-active TiO₂-based photocatalysts by carbon and nitrogen doping. *J. Catal.* **260**, 128–133 (2008)
 100. D. Jiang, Y. Xu, D. Wu, Y. Sun, Isocyanate-modified TiO₂ visible-light-activated photocatalyst. *Appl. Catal. B* **88**, 165–172 (2009)
 101. K. Villa, A. Black, X. Domenech, J. Peral, Nitrogen doped TiO₂ for hydrogen production under visible light irradiation. *Sol. Energy* **86**, 558–566 (2012)
 102. S. Qin, S.L. Chan, S. Gu, Y. Bai, Z. Ren, X. Lin, Z. Chen, W. Jia, Y. Jin, Y. Guo, Camrelizumab plus rivoceranib versus sorafenib as first-line therapy for unresectable hepatocellular carcinoma (CARES-310): a randomised, open-label, international phase 3 study. *The Lancet* **402**, 1133–1146 (2023)
 103. Y. Zou, S. Wang, An investigation of active sites for electrochemical CO₂ reduction reactions: from in situ characterization to rational design. *Adv. Sci.* **8**, 2003579 (2021)
 104. M. Dunwell, W. Luc, Y. Yan, F. Jiao, B. Xu, Understanding surface-mediated electrochemical reactions: CO₂ reduction and beyond. *ACS Catal.* **8**, 8121–8129 (2018)
 105. A.J. Morris, G.J. Meyer, E. Fujita, Molecular approaches to the photocatalytic reduction of carbon dioxide for solar fuels. *Acc. Chem. Res.* **42**, 1983–1994 (2009)
 106. Z. Yu, K. Zheng, X. Li, P. Xia, J. Xu, J. Sun, N. Zhou, F. Pan, Effect of Ti6Al4V reinforcement particles on the mechanical, wear, and corrosion properties of AZ91D magnesium matrix composites. *J. Market. Res.* **26**, 7395–7411 (2023)
 107. I. Willner, R. Moidan, D. Mandler, H. Duerr, G. Doerr, K. Zengerle, Photosensitized reduction of carbon dioxide to methane and hydrogen evolution in the presence of ruthenium and osmium colloids: strategies to design selectivity of products distribution. *J. Am. Chem. Soc.* **109**, 6080–6086 (1987)
 108. A. Yahaya, M. Gondal, A. Hameed, Selective laser enhanced photocatalytic conversion of CO₂ into methanol. *Chem. Phys. Lett.* **400**, 206–212 (2004)
 109. W.A. Thompson, E. Sanchez Fernandez, M.M. Maroto-Valer, Review and analysis of CO₂ photoreduction kinetics. *ACS Sustain. Chem. Eng.* **8**, 4677–4692 (2020)
 110. M. Tahir, N.S. Amin, Photocatalytic CO₂ reduction with H₂O vapors using montmorillonite/TiO₂ supported microchannel monolith photoreactor. *Chem. Eng. J.* **230**, 314–327 (2013)
 111. L.-L. Tan, W.-J. Ong, S.-P. Chai, A.R. Mohamed, Photocatalytic reduction of CO₂ with H₂O over graphene oxide-supported oxygen-rich TiO₂ hybrid photocatalyst under visible light irradiation: process and kinetic studies. *Chem. Eng. J.* **308**, 248–255 (2017)
 112. A. Khalilzadeh, A. Shariati, Photoreduction of CO₂ over heterogeneous modified TiO₂ nanoparticles under visible light irradiation: synthesis, process and kinetic study. *Sol. Energy* **164**, 251–261 (2018)
 113. S. Delavari, N.A.S. Amin, Photocatalytic conversion of CO₂ and CH₄ over immobilized titania nanoparticles coated on mesh: optimization and kinetic study. *Appl. Energy* **162**, 1171–1185 (2016)
 114. M. Tahir, N.S. Amin, Indium-doped TiO₂ nanoparticles for photocatalytic CO₂ reduction with H₂O vapors to CH₄. *Appl. Catal. B* **162**, 98–109 (2015)
 115. J.C. Wu, H.-M. Lin, C.-L. Lai, Photo reduction of CO₂ to methanol using optical-fiber photoreactor. *Appl. Catal. A* **296**, 194–200 (2005)
 116. Y. Ku, W.-H. Lee, W.-Y. Wang, Photocatalytic reduction of carbonate in aqueous solution by UV/TiO₂ process. *J. Mol. Catal. A: Chem.* **212**, 191–196 (2004)
 117. S. Jain, G. Dangi, J. Vardia, S.C. Ameta, Photocatalytic reduction of some alkali carbonates in the presence of methylene blue. *Int. J. Energy Res.* **23**, 71–77 (1999)
 118. J. Ran, M. Jaroniec, S.Z. Qiao, Cocatalysts in semiconductor-based photocatalytic CO₂ reduction: achievements, challenges, and opportunities. *Adv. Mater.* **30**, 1704649 (2018)
 119. J. Ângelo, L. Andrade, L.M. Madeira, A. Mendes, An overview of photocatalysis phenomena applied to NO_x abatement. *J. Environ. Manag.* **129**, 522–539 (2013)
 120. H. Chen, C.E. Nanayakkara, V.H. Grassian, Titanium dioxide photocatalysis in atmospheric chemistry. *Chem. Rev.* **112**, 5919–5948 (2012)
 121. S. Nahar, M. Zain, A.A.H. Kadhum, H.A. Hasan, M.R. Hasan, Advances in photocatalytic CO₂ reduction with water: a review. *Materials* **10**, 629 (2017)
 122. J.M. Luo, C.F. Lam, Travel anxiety, risk attitude and travel intentions towards “travel bubble” destinations in Hong Kong: effect of the fear of COVID-19. *Int. J. Environ. Res. Public Health* **17**, 7859 (2020)
 123. M. Cheng, P. He, L. Lei, X. Tan, X. Wang, Y. Sun, J. Li, Y. Jiang, Comparative studies on microstructure evolution and corrosion resistance of 304 and a newly developed high Mn and N austenitic stainless steel welded joints. *Corros. Sci.* **183**, 109338 (2021)
 124. W. Fan, Q. Zhang, Y. Wang, Semiconductor-based nanocomposites for photocatalytic H₂ production and CO₂ conversion. *Phys. Chem. Chem. Phys.* **15**, 2632–2649 (2013)
 125. S. Shen, J. Shi, P. Guo, L. Guo, Visible-light-driven photocatalytic water splitting on nanostructured semiconducting materials. *Int. J. Nanotechnol.* **8**, 523–591 (2011)
 126. P. Rajesh, F.H. Shajin, B.N. Kommula, An efficient integration and control approach to increase the conversion efficiency of high-current low-voltage DC/DC converter. *Energy Syst.* **13**, 939–958 (2022)
 127. J. Yu, J. Jin, B. Cheng, M. Jaroniec, A noble metal-free reduced graphene oxide–CdS nanorod composite for the enhanced visible-light photocatalytic reduction of CO₂ to solar fuel. *J. Mater. Chem. A* **2**, 3407–3416 (2014)
 128. J. Lin, Z. Pan, X. Wang, Photochemical reduction of CO₂ by graphitic carbon nitride polymers. *ACS Sustain. Chem. Eng.* **2**, 353–358 (2014)
 129. J. Yu, K. Wang, W. Xiao, B. Cheng, Photocatalytic reduction of CO₂ into hydrocarbon solar fuels over gC₃N₄–Pt nanocomposite photocatalysts. *Phys. Chem. Chem. Phys.* **16**, 11492–11501 (2014)
 130. Y. Liu, Z. Wang, B. Huang, Y. Dai, X. Qin, X. Zhang, Microstructure modulation of semiconductor photocatalysts for CO₂ reduction. *Curr. Org. Chem.* **18**, 620–628 (2014)
 131. Y.P. Xie, G. Liu, L. Yin, H.-M. Cheng, Crystal facet-dependent photocatalytic oxidation and reduction reactivity of monoclinic WO₃ for solar energy conversion. *J. Mater. Chem.* **22**, 6746–6751 (2012)
 132. Y. Matsumoto, Energy positions of oxide semiconductors and photocatalysis with iron complex oxides. *J. Solid State Chem.* **126**, 227–234 (1996)
 133. L. Jia, J. Li, W. Fang, Enhanced visible-light active C and Fe codoped LaCoO₃ for reduction of carbon dioxide. *Catal. Commun.* **11**, 87–90 (2009)
 134. Y. Liu, B. Huang, Y. Dai, X. Zhang, X. Qin, M. Jiang, M.-H. Whangbo, Selective ethanol formation from photocatalytic reduction of carbon dioxide in water with BiVO₄ photocatalyst. *Catal. Commun.* **11**, 210–213 (2009)
 135. J. Mao, T. Peng, X. Zhang, K. Li, L. Zan, Selective methanol production from photocatalytic reduction of CO₂ on BiVO₄ under visible light irradiation. *Catal. Commun.* **28**, 38–41 (2012)
 136. Y. Zhou, Z. Tian, Z. Zhao, Q. Liu, J. Kou, X. Chen, J. Gao, S. Yan, Z. Zou, High-yield synthesis of ultrathin and uniform Bi₂WO₆

- square nanoplates benefitting from photocatalytic reduction of CO₂ into renewable hydrocarbon fuel under visible light. *ACS Appl. Mater. Interfaces* **3**, 3594–3601 (2011)
137. H. Cheng, B. Huang, Y. Liu, Z. Wang, X. Qin, X. Zhang, Y. Dai, An anion exchange approach to Bi₂WO₆ hollow microspheres with efficient visible light photocatalytic reduction of CO₂ to methanol. *Chem. Commun.* **48**, 9729–9731 (2012)
 138. P. Li, Y. Zhou, W. Tu, Q. Liu, S. Yan, Z. Zou, Direct growth of Fe₂V₄O₁₃ nanoribbons on a stainless-steel mesh for visible-light photoreduction of CO₂ into renewable hydrocarbon fuel and degradation of gaseous isopropyl alcohol. *ChemPlusChem* **78**, 274–278 (2013)
 139. Z.-Y. Wang, H.-C. Chou, J.C. Wu, D.P. Tsai, G. Mul, CO₂ photoreduction using NiO/InTaO₄ in optical-fiber reactor for renewable energy. *Appl. Catal. A* **380**, 172–177 (2010)
 140. P.-W. Pan, Y.-W. Chen, Photocatalytic reduction of carbon dioxide on NiO/InTaO₄ under visible light irradiation. *Catal. Commun.* **8**, 1546–1549 (2007)
 141. H.-C. Chen, H.-C. Chou, J.C. Wu, H.-Y. Lin, Sol–gel prepared InTaO₄ and its photocatalytic characteristics. *J. Mater. Res.* **23**, 1364–1370 (2008)
 142. C.-W. Tsai, H.M. Chen, R.-S. Liu, K. Asakura, T.-S. Chan, Ni@NiO core–shell structure-modified nitrogen-doped InTaO₄ for solar-driven highly efficient CO₂ reduction to methanol. *J. Phys. Chem. C* **115**, 10180–10186 (2011)
 143. W. Shi, M. Laabs, M. Reinmoeller, L. Kong, S.V. Vassilev, S. Guhl, J. Bai, B. Meyer, W. Li, The fusion mechanism of complex minerals mixture and prediction model for flow temperature of coal ash for gasification. *Fuel* **305**, 121448 (2021)
 144. S. Li, Y. Wu, H. Zheng, H. Li, Y. Zheng, J. Nan, J. Ma, D. Nagarajan, J.-S. Chang, Antibiotics degradation by advanced oxidation process (AOPs): recent advances in ecotoxicity and antibiotic-resistance genes induction of degradation products. *Chemosphere* **311**, 136977 (2023)
 145. N. Serpone, A. Emeline, *Semiconductor Photocatalysis—Past, Present, and Future Outlook* (ACS Publications, London, 2012), pp.673–677
 146. J.-X. Wang, Y. Zhao, M.-S. Chen, H. Zhang, J.-G. Cui, J.-L. Li, Heme-oxygenase-1 as a target for phthalate-induced cardiomyocytes ferroptosis. *Environ. Pollut.* **317**, 120717 (2023)
 147. L.G. Devi, R. Kavitha, A review on non metal ion doped titania for the photocatalytic degradation of organic pollutants under UV/solar light: role of photogenerated charge carrier dynamics in enhancing the activity. *Appl. Catal. B* **140**, 559–587 (2013)
 148. R. Huang, J. Wu, M. Zhang, B. Liu, Z. Zheng, D. Luo, Strategies to enhance photocatalytic activity of graphite carbon nitride-based photocatalysts. *Mater. Des.* **210**, 110040 (2021)
 149. F.A. Qaraah, S.A. Mahyoub, Q.A. Drmash, A. Qaraah, F. Xin, One-step fabrication of unique 3D/2D S, O-doped g-C₃N₄ S-scheme isotype heterojunction for boosting CO₂ photoreduction. *Mater. Today Sustain.* **23**, 100437 (2023)
 150. N. Serpone, *Is the Band Gap of Pristine TiO₂ Narrowed by Anion-and Cation-Doping of Titanium Dioxide in Second-Generation Photocatalysts?* (ACS Publications, London, 2006), pp. 24287–24293.
 151. S.B. Patil, P.S. Basavarajappa, N. Ganganagappa, M. Jyothi, A. Raghur, K.R. Reddy, Recent advances in non-metals-doped TiO₂ nanostructured photocatalysts for visible-light driven hydrogen production, CO₂ reduction and air purification. *Int. J. Hydrog. Energy* **44**, 13022–13039 (2019)
 152. N. Shehzad, M. Tahir, K. Johari, T. Murugesan, M. Hussain, A critical review on TiO₂ based photocatalytic CO₂ reduction system: strategies to improve efficiency. *J. CO₂ Util.* **26**, 98–122 (2018).
 153. Y. Yan, Y. Yu, S. Huang, Y. Yang, X. Yang, S. Yin, Y. Cao, Adjustment and matching of energy band of TiO₂-based photocatalysts by metal ions (Pd, Cu, Mn) for photoreduction of CO₂ into CH₄. *J. Phys. Chem. C* **121**, 1089–1098 (2017)
 154. Y. Sohn, W. Huang, F. Taghipour, Recent progress and perspectives in the photocatalytic CO₂ reduction of Ti-oxide-based nanomaterials. *Appl. Surf. Sci.* **396**, 1696–1711 (2017)
 155. J. Jiao, Y. Wei, K. Chi, Z. Zhao, A. Duan, J. Liu, G. Jiang, Y. Wang, X. Wang, C. Han, Platinum nanoparticles supported on TiO₂ photonic crystals as highly active photocatalyst for the reduction of CO₂ in the presence of water. *Energ. Technol.* **5**, 877–883 (2017)
 156. M. Tahir, B. Tahir, N.A.S. Amin, H. Alias, Selective photocatalytic reduction of CO₂ by H₂O/H₂ to CH₄ and CH₃OH over Cu-promoted In₂O₃/TiO₂ nanocatalyst. *Appl. Surf. Sci.* **389**, 46–55 (2016)
 157. B. Yu, Y. Zhou, P. Li, W. Tu, P. Li, L. Tang, J. Ye, Z. Zou, Photocatalytic reduction of CO₂ over Ag/TiO₂ nanocomposites prepared with a simple and rapid silver mirror method. *Nanoscale* **8**, 11870–11874 (2016)
 158. M. Tahir, B. Tahir, N.A.S. Amin, A. Muhammad, Photocatalytic CO₂ methanation over NiO/In₂O₃ promoted TiO₂ nanocatalysts using H₂O and/or H₂ reductants. *Energy Convers. Manag.* **119**, 368–378 (2016)
 159. X. Meng, S. Ouyang, T. Kako, P. Li, Q. Yu, T. Wang, J. Ye, Photocatalytic CO₂ conversion over alkali modified TiO₂ without loading noble metal cocatalyst. *Chem. Commun.* **50**, 11517–11519 (2014)
 160. L. Collado, A. Reynal, J. Coronado, D. Serrano, J. Durrant, V. De la Peña O'Shea, Effect of Au surface plasmon nanoparticles on the selective CO₂ photoreduction to CH₄. *Appl. Catal. B Environ.* **178**, 177–185 (2015).
 161. Y. Kohno, H. Hayashi, S. Takenaka, T. Tanaka, T. Funabiki, S. Yoshida, Photo-enhanced reduction of carbon dioxide with hydrogen over Rh/TiO₂. *J. Photochem. Photobiol. A* **126**, 117–123 (1999)
 162. Y.T. Liang, B.K. Vijayan, O. Lyandres, K.A. Gray, M.C. Hersam, Effect of dimensionality on the photocatalytic behavior of carbon–titania nanosheet composites: charge transfer at nanomaterial interfaces. *J. Phys. Chem. Lett.* **3**, 1760–1765 (2012)
 163. J.F. de Brito, M.V.B. Zanoni, On the application of Ti/TiO₂/CuO np junction semiconductor: a case study of electrolyte, temperature and potential influence on CO₂ reduction. *Chem. Eng. J.* **318**, 264–271 (2017)
 164. J. Fan, E.-Z. Liu, L. Tian, X.-Y. Hu, Q. He, T. Sun, Synergistic effect of N and Ni²⁺ on nanotitania in photocatalytic reduction of CO₂. *J. Environ. Eng.* **137**, 171–176 (2011)
 165. A. Sharma, B.-K. Lee, Photocatalytic reduction of carbon dioxide to methanol using nickel-loaded TiO₂ supported on activated carbon fiber. *Catal. Today* **298**, 158–167 (2017)
 166. X. Li, Q. Wang, Y. Zhao, W. Wu, J. Chen, H. Meng, Green synthesis and photo-catalytic performances for ZnO-reduced graphene oxide nanocomposites. *J. Colloid Interface Sci.* **411**, 69–75 (2013)
 167. Q. Zhang, C.-F. Lin, Y.H. Jing, C.-T. Chang, Photocatalytic reduction of carbon dioxide to methanol and formic acid by graphene-TiO₂. *J. Air Waste Manag. Assoc.* **64**, 578–585 (2014)
 168. K. Thamaraiselvi, T. Sivakumar, Photocatalytic reduction of carbon dioxide by using bare and copper oxide impregnated nano titania catalysts. *J. Nanosci. Nanotechnol.* **17**, 313–322 (2017)
 169. T. Zhang, J. Low, X. Huang, J.F. Al-Sharab, J. Yu, T. Asefa, Copper-decorated microsized nanoporous titanium dioxide photocatalysts for carbon dioxide reduction by water. *ChemCatChem* **9**, 3054–3062 (2017)
 170. G. Xi, S. Ouyang, P. Li, J. Ye, Q. Ma, N. Su, H. Bai, C. Wang, Ultrathin W18O₄₉ nanowires with diameters below 1 nm: synthesis, near-infrared absorption, photoluminescence, and

- photochemical reduction of carbon dioxide. *Angew. Chem. Int. Ed.* **51**, 2395–2399 (2012)
171. X. Pan, M.-Q. Yang, X. Fu, N. Zhang, Y.-J. Xu, Defective TiO₂ with oxygen vacancies: synthesis, properties and photocatalytic applications. *Nanoscale* **5**, 3601–3614 (2013)
 172. M. Huang, T. Tang, P. Pang, M. Li, R. Ma, J. Lu, J. Shu, Y. You, B. Chen, J. Liang, Treating COVID-19 with chloroquine. *J. Mol. Cell Biol.* **12**, 322–325 (2020)
 173. L. Liu, H. Zhao, J.M. Andino, Y. Li, Photocatalytic CO₂ reduction with H₂O on TiO₂ nanocrystals: comparison of anatase, rutile, and brookite polymorphs and exploration of surface chemistry. *ACS Catal.* **2**, 1817–1828 (2012)
 174. D.R. Eddy, M.D. Permana, L.K. Sakti, G.A.N. Sheha, Solihudin, S. Hidayat, T. Takei, N. Kumada, I. Rahayu, Heterophase polymorph of TiO₂ (Anatase, Rutile, Brookite, TiO₂ (B)) for efficient photocatalyst: fabrication and activity. *Nanomaterials* **13** (2023) 704.
 175. G. Tompsett, G. Bowmaker, R. Cooney, J. Metson, K. Rodgers, J. Seakins, The Raman spectrum of brookite, TiO₂ (PBCA, Z = 8). *J. Raman Spectrosc.* **26**, 57–62 (1995)
 176. A. Beltran, L. Gracia, J. Andres, Density functional theory study of the brookite surfaces and phase transitions between natural titania polymorphs. *J. Phys. Chem. B* **110**, 23417–23423 (2006)
 177. Z. Li, S. Cong, Y. Xu, Brookite vs anatase TiO₂ in the photocatalytic activity for organic degradation in water. *ACS Catal.* **4**, 3273–3280 (2014)
 178. Z. Zhang, Y. Li, J. Shi, L. Zhu, Y. Dai, P. Fu, S. Liu, M. Hong, J. Zhang, J. Wang, Lymphocyte-related immunomodulatory therapy with siponimod (BAF-312) improves outcomes in mice with acute intracerebral hemorrhage. *Aging Dis.* **14**, 966 (2023)
 179. B.A. Malla, S. Ramanjeneya, J. Vergis, S.S. Malik, S.B. Barbudde, D.B. Rawool, Comparison of recombinant and synthetic listeriolysin-O peptide-based indirect ELISA vis-à-vis cultural isolation for detection of listeriosis in caprine and ovine species. *J. Microbiol. Methods* **188**, 106278 (2021)
 180. A.S. Malik, H. Bali, F. Czirok, Á. Szamosvölgyi, G. Halasi, A. Efreмова, B. Šmíd, A. Sápi, Á. Kukovecz, Z. Kónya, Turning CO₂ to CH₄ and CO over CeO₂ and MCF-17 supported Pt, Ru and Rh nanoclusters—influence of nanostructure morphology, supporting materials and operating conditions. *Fuel* **326**, 124994 (2022)
 181. F. Bibi, M.I. Ali, M. Ahmad, A. Bokhari, K.S. Khoo, M. Zafar, S. Asif, M. Mubashir, N. Han, P.L. Show, Production of lipids biosynthesis from *Tetrademus nygaardii* microalgae as a feedstock for biodiesel production. *Fuel* **326**, 124985 (2022)
 182. K.S. Novoselov, A.K. Geim, S.V. Morozov, D.-E. Jiang, Y. Zhang, S.V. Dubonos, I.V. Grigorieva, A.A. Firsov, Electric field effect in atomically thin carbon films. *Science* **306**, 666–669 (2004)
 183. A.K. Geim, K.S. Novoselov, The rise of graphene. *Nat. Mater.* **6**, 183–191 (2007)
 184. K. Thodkar, F. Gramm, Enhanced mobility in suspended chemical vapor-deposited graphene field-effect devices in ambient conditions. *ACS Appl. Mater. Interfaces* **15**, 37756–37763 (2023)
 185. C. Shu, H.-Y. Zhao, S. Zhao, W. Deng, P. Min, X.-H. Lu, X. Li, Z.-Z. Yu, Highly thermally conductive phase change composites with anisotropic graphene/cellulose nanofiber hybrid aerogels for efficient temperature regulation and solar-thermal-electric energy conversion applications. *Compos. B Eng.* **248**, 110367 (2023)
 186. A.R. Urade, I. Lahiri, K. Suresh, Graphene properties, synthesis and applications: a review. *JOM* **75**, 614–630 (2023)
 187. R. Wazalwar, M. Sahu, *Novel Applications of Graphene in the Aerospace Industry, Novel Applications of Carbon Based Nano-Materials* (CRC Press, Boca Raton, 2022), pp.180–198
 188. A. Armano, S. Agnello, Two-dimensional carbon: a review of synthesis methods, and electronic, optical, and vibrational properties of single-layer graphene. *C* **5**, 67 (2019)
 189. S. Chakraborty, R. Saha, S. Saha, A critical review on graphene and graphene-based derivatives from natural sources emphasizing on CO₂ adsorption potential. *Environ. Sci. Pollut. Res.* **2023**, 1–31 (2023)
 190. S.-Y. Lee, S.-J. Park, A review on solid adsorbents for carbon dioxide capture. *J. Ind. Eng. Chem.* **23**, 1–11 (2015)
 191. N.A.F. Mazri, A. Arifutzzaman, M.K. Aroua, M.E. Rahman, S.A. Mazari, Graphene and its tailoring as emerging 2D nanomaterials in efficient CO₂ absorption: a state-of-the-art interpretative review. *Alex. Eng. J.* **77**, 479–502 (2023)
 192. A. Ghosh, K. Subrahmanyam, K.S. Krishna, S. Datta, A. Govindaraj, S.K. Pati, C. Rao, Uptake of H₂ and CO₂ by graphene. *J. Phys. Chem. C* **112**, 15704–15707 (2008)
 193. L. Ekhlasi, H. Younesi, A. Rashidi, N. Bahramifar, Populus wood biomass-derived graphene for high CO₂ capture at atmospheric pressure and estimated cost of production. *Process. Saf. Environ. Prot.* **113**, 97–108 (2018)
 194. M.O. Aquatar, J.S. Mankar, U. Bhatia, S.S. Rayalu, R.J. Krupadam, Graphene nanosheets from hazardous/solid wastes: an efficient CO₂ capture material. *J. Environ. Chem. Eng.* **9**, 105839 (2021)
 195. S. Chowdhury, R. Balasubramanian, Highly efficient, rapid and selective CO₂ capture by thermally treated graphene nanosheets. *J. CO₂ Util.* **13** (2016) 50–60.
 196. L.-Y. Meng, S.-J. Park, Effect of exfoliation temperature on carbon dioxide capture of graphene nanoplates. *J. Colloid Interface Sci.* **386**, 285–290 (2012)
 197. J. Pokhrel, N. Bhorla, S. Anastasiou, T. Tsoufis, D. Gournis, G. Romanos, G.N. Karanikolos, CO₂ adsorption behavior of amine-functionalized ZIF-8, graphene oxide, and ZIF-8/graphene oxide composites under dry and wet conditions. *Microporous Mesoporous Mater.* **267**, 53–67 (2018)
 198. N. Politakos, I. Barbarin, L.S. Cantador, J.A. Cecilia, E. Mehravar, R. Tomovska, Graphene-based monolithic nanostructures for CO₂ capture. *Ind. Eng. Chem. Res.* **59**, 8612–8621 (2020)
 199. M. Aggarwal, S. Basu, N.P. Shetti, M.N. Nadagouda, T.M. Aminabhavi, Photocatalytic conversion of CO₂ into valuable products using emerging two-dimensional graphene-based nanomaterials: a step towards sustainability. *Chem. Eng. J.* **425**, 131401 (2021)
 200. Y. Kuang, J. Shang, T. Zhu, Photoactivated graphene oxide to enhance photocatalytic reduction of CO₂. *ACS Appl. Mater. Interfaces* **12**, 3580–3591 (2019)
 201. X. Wang, K. Li, J. He, J. Yang, F. Dong, W. Mai, M. Zhu, Defect in reduced graphene oxide tailored selectivity of photocatalytic CO₂ reduction on Cs₄PbBr₆ perovskite hole-in-microdisk structure. *Nano Energy* **78**, 105388 (2020)
 202. P. Devi, J. Singh, Visible light induced selective photocatalytic reduction of CO₂ to CH₄ on In₂O₃-rGO nanocomposites. *J. CO₂ Util.* **43** (2021) 101376.
 203. L.-Y. Lin, Y. Nie, S. Kavadiya, T. Soundappan, P. Biswas, N-doped reduced graphene oxide promoted nano TiO₂ as a bifunctional adsorbent/photocatalyst for CO₂ photoreduction: Effect of N species. *Chem. Eng. J.* **316**, 449–460 (2017)
 204. C. Bie, B. Zhu, F. Xu, L. Zhang, J. Yu, In situ grown monolayer N-doped graphene on CdS hollow spheres with seamless contact for photocatalytic CO₂ reduction. *Adv. Mater.* **31**, 1902868 (2019)
 205. C.B. Hiragond, J. Lee, H. Kim, J.-W. Jung, C.-H. Cho, S.-I. In, A novel N-doped graphene oxide enfolded reduced titania for highly stable and selective gas-phase photocatalytic CO₂ reduction into CH₄: an in-depth study on the interfacial charge transfer mechanism. *Chem. Eng. J.* **416**, 127978 (2021)

206. M.R.U.D. Biswas, A. Ali, K.Y. Cho, W.-C. Oh, Novel synthesis of WSe₂-graphene-TiO₂ ternary nanocomposite via ultrasonic technics for high photocatalytic reduction of CO₂ into CH₃OH. *Ultrason. Sonochem.* **42**, 738–746 (2018)
207. L. Zhang, N. Li, H. Jiu, G. Qi, Y. Huang, ZnO-reduced graphene oxide nanocomposites as efficient photocatalysts for photocatalytic reduction of CO₂. *Ceram. Int.* **41**, 6256–6262 (2015)
208. J.O. Olowoyo, M. Kumar, B. Singh, V.O. Oninla, J.O. Babalola, H. Valdés, A.V. Vorontsov, U. Kumar, Self-assembled reduced graphene oxide-TiO₂ nanocomposites: synthesis, DFTB+ calculations, and enhanced photocatalytic reduction of CO₂ to methanol. *Carbon* **147**, 385–397 (2019)
209. W.-J. Ong, L.-L. Tan, S.-P. Chai, S.-T. Yong, Graphene oxide as a structure-directing agent for the two-dimensional interface engineering of sandwich-like graphene-g-C₃N₄ hybrid nanostructures with enhanced visible-light photoreduction of CO₂ to methane. *Chem. Commun.* **51**, 858–861 (2015)
210. Z. Tong, D. Yang, J. Shi, Y. Nan, Y. Sun, Z. Jiang, Three-dimensional porous aerogel constructed by g-C₃N₄ and graphene oxide nanosheets with excellent visible-light photocatalytic performance. *ACS Appl. Mater. Interfaces* **7**, 25693–25701 (2015)
211. W.-J. Ong, L.-L. Tan, S.-P. Chai, S.-T. Yong, A.R. Mohamed, Surface charge modification via protonation of graphitic carbon nitride (g-C₃N₄) for electrostatic self-assembly construction of 2D/2D reduced graphene oxide (rGO)/g-C₃N₄ nanostructures toward enhanced photocatalytic reduction of carbon dioxide to methane. *Nano Energy* **13**, 757–770 (2015)
212. C. Han, Y. Lei, B. Wang, Y. Wang, In situ-fabricated 2D/2D heterojunctions of ultrathin SiC/reduced graphene oxide nanosheets for efficient CO₂ photoreduction with high CH₄ selectivity. *ChemSuschem* **11**, 4237–4245 (2018)
213. A. Bafaqeer, M. Tahir, N.A.S. Amin, Synergistic effects of 2D/2D ZnV₂O₆/RGO nanosheets heterojunction for stable and high performance photo-induced CO₂ reduction to solar fuels. *Chem. Eng. J.* **334**, 2142–2153 (2018)
214. Z. Otgonbayar, K.Y. Cho, W.-C. Oh, Enhanced photocatalytic activity of CO₂ reduction to methanol through the use of a novel-structured CuCaAg₂Se-graphene-TiO₂ ternary nanocomposite. *New J. Chem.* **44**, 16795–16809 (2020)
215. Z. Otgonbayar, Y. Liu, K.Y. Cho, C.-H. Jung, W.-C. Oh, Novel ternary composite of LaYAgO₄ and TiO₂ united with graphene and its complement: Photocatalytic performance of CO₂ reduction into methanol. *Mater. Sci. Semicond. Process.* **121**, 105456 (2021)
216. X. Chang, T. Wang, J. Gong, CO₂ photo-reduction: insights into CO₂ activation and reaction on surfaces of photocatalysts. *Energy Environ. Sci.* **9**, 2177–2196 (2016)
217. S. Xie, Q. Zhang, G. Liu, Y. Wang, Photocatalytic and photoelectrocatalytic reduction of CO₂ using heterogeneous catalysts with controlled nanostructures. *Chem. Commun.* **52**, 35–59 (2016)
218. C.-W. Huang, V.-H. Nguyen, S.-R. Zhou, S.-Y. Hsu, J.-X. Tan, K.C.-W. Wu, Metal-organic frameworks: preparation and applications in highly efficient heterogeneous photocatalysis. *Sustain. Energy Fuels* **4**, 504–521 (2020)
219. Q. Chen, S. Sun, Y. Wang, Q. Zhang, L. Zhu, Y. Liu, In-situ remediation of phosphogypsum in a cement-free pathway: utilization of ground granulated blast furnace slag and NaOH pretreatment. *Chemosphere* **313**, 137412 (2023)
220. Z. Zhang, Y. Zheng, L. Qian, D. Luo, H. Dou, G. Wen, A. Yu, Z. Chen, Emerging trends in sustainable CO₂-management materials. *Adv. Mater.* **34**, 2201547 (2022)
221. S. Wang, M. Xu, T. Peng, C. Zhang, T. Li, I. Hussain, J. Wang, B. Tan, Porous hypercrosslinked polymer-TiO₂-graphene composite photocatalysts for visible-light-driven CO₂ conversion. *Nat. Commun.* **10**, 676 (2019)
222. S. Wang, K. Song, C. Zhang, Y. Shu, T. Li, B. Tan, A novel metalporphyrin-based microporous organic polymer with high CO₂ uptake and efficient chemical conversion of CO₂ under ambient conditions. *J. Mater. Chem. A* **5**, 1509–1515 (2017)
223. K. Yuan, Y. Xu, J. Uihlein, G. Brunklaus, L. Shi, R. Heiderhoff, M. Que, M. Forster, T. Chassé, T. Pichler, Straightforward generation of pillared, microporous graphene frameworks for use in supercapacitors. *Adv. Mater.* **27**, 6714–6721 (2015)
224. S. Wang, C. Zhang, Y. Shu, S. Jiang, Q. Xia, L. Chen, S. Jin, I. Hussain, A.I. Cooper, B. Tan, Layered microporous polymers by solvent knitting method. *Sci. Adv.* **3**, e1602610 (2017)
225. Y. Liu, S. Wang, X. Meng, Y. Ye, X. Song, Z. Liang, Increasing the surface area and CO₂ uptake of conjugated microporous polymers via a post-knitting method. *Mater. Chem. Frontiers* **5**, 5319–5327 (2021)
226. Y. Sun, C. Liu, W. Su, Y. Zhou, L. Zhou, Principles of methane adsorption and natural gas storage. *Adsorption* **15**, 133–137 (2009)
227. Z. Xu, C. Zhuang, Z. Zou, J. Wang, X. Xu, T. Peng, Enhanced photocatalytic activity by the construction of a TiO₂/carbon nitride nanosheets heterostructure with high surface area via direct interfacial assembly. *Nano Res.* **10**, 2193–2209 (2017)
228. J. Wang, L. Huang, R. Yang, Z. Zhang, J. Wu, Y. Gao, Q. Wang, D. O'Hare, Z. Zhong, Recent advances in solid sorbents for CO₂ capture and new development trends. *Energy Environ. Sci.* **7**, 3478–3518 (2014)
229. L. Tan, B. Tan, Hypercrosslinked porous polymer materials: design, synthesis, and applications. *Chem. Soc. Rev.* **46**, 3322–3356 (2017)
230. X. Yang-Fan, Y. Mu-Zi, C. Bai-Xue, W. Xu-Dong, C. Hong-Yan, K. Dai-Bin, S. Cheng-Yong, A CsPbBr₃ perovskite quantum dot/graphene oxide composite for photocatalytic CO₂ reduction (2017).
231. Z. Gu, B. Zhang, Y. Asakura, S. Tsukuda, H. Kato, M. Kaki-hana, S. Yin, Alkali-assisted hydrothermal preparation of g-C₃N₄/rGO nanocomposites with highly enhanced photocatalytic NO_x removal activity. *Appl. Surf. Sci.* **521**, 146213 (2020)
232. A. Kumar, K. Sharma, M. Thakur, D. Pathania, A. Sharma, Fabrication of high visible light active LaFeO₃/Cl-g-C₃N₄/RGO heterojunction for solar assisted photo-degradation of aceclofenac. *J. Environ. Chem. Eng.* **10**, 108098 (2022)
233. Z. Zhan, H. Wang, Q. Huang, S. Li, X. Yi, Q. Tang, J. Wang, B. Tan, Grafting hypercrosslinked polymers on TiO₂ surface for anchoring ultrafine Pd nanoparticles: dramatically enhanced efficiency and selectivity toward photocatalytic reduction of CO₂ to CH₄. *Small* **18**, 2105083 (2022)
234. G.E. Schukraft, R.T. Woodward, S. Kumar, M. Sachs, S. Eslava, C. Petit, Hypercrosslinked polymers as a photocatalytic platform for visible-light-driven CO₂ photoreduction using H₂O. *ChemSuschem* **14**, 1720–1727 (2021)
235. T. Garg, A. Goyal, A. Kaushik, S. Singhal, State-of-the-art evolution of g-C₃N₄ based Z-scheme heterostructures towards energy and environmental applications: a review. *Mater. Res. Bull.* **2023**, 11248 (2023)
236. M. Mirzaei, A.H. Rasouli, A. Saedi, HOMO-LUMO photosensitization analyses of coronene-cytosine complexes. *Main Group Chem.* **20**, 565–573 (2021)
237. K. Suenaga, A. Watanabe, K. Tanaka, Y. Chujo, Design for a pure-blue-emissive polymer film through the selective perturbation of the energy level of the highest occupied molecular orbital in a boron complex. *Macromolecules* **56**, 6419–6425 (2023)
238. Y. Chai, Y. Kong, M. Lin, W. Lin, J. Shen, J. Long, R. Yuan, W. Dai, X. Wang, Z. Zhang, Metal to non-metal sites of metallic sulfides switching products from CO to CH₄ for photocatalytic CO₂ reduction. *Nat. Commun.* **14**, 6168 (2023)

239. H. Hu, Y. He, H. Yu, D. Li, M. Sun, Y. Feng, C. Zhang, H. Chen, C. Deng, Constructing a noble-metal-free 0D/2D CdS/SnS₂ heterojunction for efficient visible-light-driven photocatalytic pollutant degradation and hydrogen generation. *Nanotechnology* **34**, 505712 (2023)
240. F. Zhang, Y.-H. Li, M.-Y. Qi, Y.M. Yamada, M. Anpo, Z.-R. Tang, Y.-J. Xu, Photothermal catalytic CO₂ reduction over nanomaterials. *Chem. Catal.* **1**, 272–297 (2021)
241. P. Netzsch, F. Pielhofer, H.A. Höpfe, From S–O–S to B–O–S to B–O–B Bridges: Ba [B (S2O₇)₂]₂ as a model system for the structural diversity in borosulfate chemistry. *Inorg. Chem.* **59**, 15180–15188 (2020)
242. H. Chen, J. Xu, H. Lin, Z. Wang, Z. Liu, Multi-cycle aqueous arsenic removal by novel magnetic n/s-doped hydrochars activated via one-pot and two-stage schemes. *Chem. Eng. J.* **429**, 132071 (2022)
243. X. Xiong, C. Mao, Z. Yang, Q. Zhang, G.I. Waterhouse, L. Gu, T. Zhang, Photocatalytic CO₂ reduction to CO over Ni single atoms supported on defect-rich zirconia. *Adv. Energy Mater.* **10**, 2002928 (2020)
244. L. Zhang, X. Yang, F. Zhang, G. Long, T. Zhang, K. Leng, Y. Zhang, Y. Huang, Y. Ma, M. Zhang, Controlling the effective surface area and pore size distribution of sp² carbon materials and their impact on the capacitance performance of these materials. *J. Am. Chem. Soc.* **135**, 5921–5929 (2013)
245. D. Sundar, C.-H. Liu, S. Anandan, J.J. Wu, Photocatalytic CO₂ conversion into solar fuels using carbon-based materials—a review. *Molecules* **28**, 5383 (2023)
246. S. Peng, J. Gao, D. Stojkov, S. Yousefi, H.U. Simon, Established and emerging roles for mitochondria in neutrophils. *Immunol. Rev.* **314**, 413–426 (2023)
247. M. Yang, P. Wang, Y. Li, S. Tang, X. Lin, H. Zhang, Z. Zhu, F. Chen, Graphene aerogel-based NiAl-LDH/g-C₃N₄ with ultratight sheet-sheet heterojunction for excellent visible-light photocatalytic activity of CO₂ reduction. *Appl. Catal. B* **306**, 121065 (2022)
248. S. Gong, M. Hou, Y. Niu, X. Teng, X. Liu, M. Xu, C. Xu, V.K.-M. Au, Z. Chen, Molybdenum phosphide coupled with highly dispersed nickel confined in porous carbon nanofibers for enhanced photocatalytic CO₂ reduction. *Chem. Eng. J.* **427**, 131717 (2022)
249. X.-Q. Zhang, W.-C. Li, A.-H. Lu, Designed porous carbon materials for efficient CO₂ adsorption and separation. *New Carbon Mater.* **30**, 481–501 (2015)
250. X.-Q. Zhang, W.-C. Li, A.-H. Lu, Designed porous carbon materials for efficient CO₂ adsorption and separation. *Carbon* **100**, 260 (2016)
251. P. Zhang, Y. Dong, Z. Ren, G. Wang, Y. Guo, C. Wang, Z. Ma, Rapid urbanization and meteorological changes are reshaping the urban vegetation pattern in urban core area: a national 315-city study in China. *Sci. Total. Environ.* **904**, 167269 (2023)
252. U. Kamran, S.-J. Park, Chemically modified carbonaceous adsorbents for enhanced CO₂ capture: a review. *J. Clean. Prod.* **290**, 125776 (2021)
253. M. Zhang, C. Lai, B. Li, F. Xu, D. Huang, S. Liu, L. Qin, X. Liu, H. Yi, Y. Fu, Insightful understanding of charge carrier transfer in 2D/2D heterojunction photocatalyst: Ni–Co layered double hydroxides deposited on ornamental g-C₃N₄ ultrathin nanosheet with boosted molecular oxygen activation. *Chem. Eng. J.* **422**, 130120 (2021)
254. K. Fan, Z. Jin, H. Yang, D. Liu, H. Hu, Y. Bi, Promotion of the excited electron transfer over Ni-and Co-sulfide co-doped g-C₃N₄ photocatalyst (g-C₃N₄/Ni_xCo_{1-x}S₂) for hydrogen production under visible light irradiation. *Sci. Rep.* **7**, 7710 (2017)
255. J. Lian, W. Liu, L. Meng, J. Wu, A. Zeb, L. Cheng, Y. Lian, H. Sun, Effects of microplastics derived from polymer-coated fertilizer on maize growth, rhizosphere, and soil properties. *J. Clean. Prod.* **318**, 128571 (2021)
256. Y. Li, Z. He, L. Liu, Y. Jiang, W.-J. Ong, Y. Duan, W. Ho, F. Dong, Inside-and-out modification of graphitic carbon nitride (g-C₃N₄) photocatalysts via defect engineering for energy and environmental science. *Nano Energy* **105**, 108032 (2023)
257. J. Wang, Y. Song, C. Zuo, R. Li, Y. Zhou, Y. Zhang, B. Wu, Few-layer porous carbon nitride anchoring Co and Ni with charge transfer mechanism for photocatalytic CO₂ reduction. *J. Colloid Interface Sci.* **625**, 722–733 (2022)
258. V.S. Vyas, V.W.-H. Lau, B.V. Lotsch, Soft photocatalysis: organic polymers for solar fuel production. *Chem. Mater.* **28**, 5191–5204 (2016)
259. T. Banerjee, F. Podjaski, J. Kröger, B.P. Biswal, B.V. Lotsch, Polymer photocatalysts for solar-to-chemical energy conversion. *Nat. Rev. Mater.* **6**, 168–190 (2021)
260. J. Hou, T. Jiang, X. Wang, G. Zhang, J.-J. Zou, C. Cao, Variable dimensional structure and interface design of g-C₃N₄/BiOI composites with oxygen vacancy for improving visible-light photocatalytic properties. *J. Clean. Prod.* **287**, 125072 (2021)
261. H. An, B. Lin, C. Xue, X. Yan, Y. Dai, J. Wei, G. Yang, Formation of BiOI/g-C₃N₄ nanosheet composites with high visible-light-driven photocatalytic activity. *Chin. J. Catal.* **39**, 654–663 (2018)
262. J. Liang, X. Li, J. Zuo, J. Lin, Z. Liu, Hybrid 0D/2D heterostructures: in-situ growth of 0D g-C₃N₄ on 2D BiOI for efficient photocatalyst. *Adv. Compos. Hybrid Mater.* **4**, 1122–1136 (2021)
263. W. Shen, Y. Lu, J.A. Hu, H. Le, W. Yu, W. Xu, W. Yu, J. Zheng, Mechanism of miR-320 in regulating biological characteristics of ischemic cerebral neuron by mediating Nox₂/ROS pathway. *J. Mol. Neurosci.* **70**, 449–457 (2020)
264. Z. You, C. Wu, Q. Shen, Y. Yu, H. Chen, Y. Su, H. Wang, C. Wu, F. Zhang, H. Yang, A novel efficient gC₃N₄@ BiOI p–n heterojunction photocatalyst constructed through the assembly of gC₃N₄ nanoparticles. *Dalton Trans.* **47**, 7353–7361 (2018)
265. F. Kuttassery, H. Kumagai, R. Kamata, Y. Ebato, M. Higashi, H. Suzuki, R. Abe, O. Ishitani, Supramolecular photocatalysts fixed on the inside of the polypyrrole layer in dye sensitized molecular photocathodes: application to photocatalytic CO₂ reduction coupled with water oxidation. *Chem. Sci.* **12**, 13216–13232 (2021)
266. D.H. Apaydin, E. Tordin, E. Portenkirchner, G. Aufischer, S. Schlager, M. Weichselbaumer, K. Oppelt, N.S. Sariciftci, Photoelectrochemical reduction of CO₂ using third-generation conjugated polymers. *ChemistrySelect* **1**, 1156–1162 (2016)
267. Z. Wang, X.-F. Zhang, L. Shu, J. Yao, Copper sulfide integrated functional cellulose hydrogel for efficient solar water purification. *Carbohydr. Polym.* **319**, 121161 (2023)
268. M.A. Rosen, Environmental sustainability tools in the biofuel industry. *Biofuel Res. J.* **5**, 751–752 (2018)
269. M. Aghbashlo, Z. Khounani, H. Hosseinzadeh-Bandbafha, V.K. Gupta, H. Amiri, S.S. Lam, T. Morosuk, M. Tabatabaei, Exergoenvironmental analysis of bioenergy systems: a comprehensive review. *Renew. Sustain. Energy Rev.* **149**, 111399 (2021)
270. M. Aghbashlo, H. Hosseinzadeh-Bandbafha, H. Shahbeik, M. Tabatabaei, The role of sustainability assessment tools in realizing bioenergy and bioproduct systems. *Biofuel Res. J.* **9**, 1697–1706 (2022)

Publisher's Note Springer Nature remains neutral with regard to jurisdictional claims in published maps and institutional affiliations.

Springer Nature or its licensor (e.g. a society or other partner) holds exclusive rights to this article under a publishing agreement with the author(s) or other rightsholder(s); author self-archiving of the accepted manuscript version of this article is solely governed by the terms of such publishing agreement and applicable law.